

Testing the growth of cosmic structures during the Dark Ages

Elena Vanetti,^{a,b,c,d} Eleonora Vanzan,^{a,b,e} Nicola Bellomo,^{a,b,f} Alvise Raccanelli^{a,b,f}

^aDipartimento di Fisica e Astronomia G. Galilei, Università degli Studi di Padova, via Marzolo 8, I-35131 Padova, Italy

^bINFN, Sezione di Padova, Via Marzolo 8, I-35131, Padova, Italy

^cInstituto de Astrofísica de Canarias (IAC), Calle Vía Láctea, S/N, E-38205, La Laguna, Tenerife, Spain

^dDepartamento de Astrofísica, Universidad de La Laguna, Avenida Francisco Sánchez, E-38205, La Laguna, Tenerife, Spain

^eSchool of Physics and Astronomy, Tel-Aviv University, Chaim Levanon St 55, Tel-Aviv 69978, Israel

^fINAF - Osservatorio Astronomico di Padova, Vicolo dell'Osservatorio 5, I-35122 Padova, Italy

E-mail: elena.vanetti@iac.es, evanzan@taux.tau.ac.il, nicola.bellomo@unipd.it, alvise.raccanelli.1@unipd.it

Abstract. Hydrogen 21-cm Line Intensity Mapping offers the unique opportunity to access the Dark Ages and trace the formation and evolution of the large scale structure of the Universe prior to star and galaxy formation. In this work we investigate the potential of future Earth- and Moon-based 21-cm surveys to constrain the growth of structures during the currently unexplored redshift range $30 < z < 200$. On the one hand we show how foreground contamination could limit the capabilities of future instruments in achieving precision below the 10% level. On the other hand, observations from the far side of the Moon have the potential to reach percent or even sub-percent precision in terms of reconstructing the growth of cosmic structures, if foregrounds are robustly accounted for. Such exquisite precision will provide tight constraints on models that induce deviations from Λ CDM, not only during the Dark Ages, but also during recombination or that manifest mostly in the low-redshift Universe, like Early Dark Energy and nDGP models, respectively. Thus, because of their insensitivity to non-linearities or astrophysical processes, line intensity mapping surveys will provide a formidable consistency check to potential claims of discoveries of new physics that affect the growth of structures.

Contents

1	Introduction	1
2	Observing the Dark Ages	2
2.1	Hydrogen 21-cm line	2
2.2	Forecasting the sensitivity of 21-cm experiments	3
3	Alternative models of structure growth	6
3.1	Model-independent approach on reconstructing growth history	6
3.2	Deviations arising during the Dark Ages	6
3.3	Late universe phenomenology	7
3.4	Deviations arising before the Dark Ages	7
4	Constraints on the growth of structure	8
5	Conclusions	12
A	The angular power spectrum of 21-cm brightness temperature fluctuations	14
B	Angular resolution in presence of foregrounds	15
C	Tables of constraints and cumulative errors	15

1 Introduction

Structure formation in the cosmological standard model, the so-called Λ CDM+General Relativity (GR), has been well understood for almost four decades [1–3]. Initial (linear) perturbations in the matter field, whose origin can be traced back to the inflationary epoch, start growing after horizon re-entry because of gravitational instability, until they become nonlinear and form virialized structures [4, 5]. In the big picture of this paradigm the only required ingredients are the presence of primordial perturbations, cold dark matter (CDM), i.e., a non-relativistic species that does not interact with baryons, and gravity.

Several Cosmic Microwave Background (CMB) experiments [6–8] have returned a clear picture of the Universe at high redshift ($z \gtrsim 10^3$), around the epoch of recombination. In particular, these experiments clarified the role of CDM in providing the potential wells into which, later in cosmic history, baryons fall. Similarly, galaxy redshift surveys at low redshift ($z \lesssim 2$) confirmed that the final outcome of the growth of structure, i.e., a cosmic web made of galaxies, filaments and voids, is fully compatible with Λ CDM+GR predictions and the initial conditions for baryons measured at recombination [9–31]. However, despite this overwhelming theoretical and experimental success, the theoretical foundations and deep explanations of the physics behind Λ CDM+GR are still lacking. Moreover, the presence of a few tensions in our current set of observations regarding the expansion history and growth of structure could hint at the presence of beyond- Λ CDM Physics [31–34].

There are theoretical models attempting to both explain the observed data and the accelerated expansion of the Universe, and to cure these tensions by extending Λ CDM, invoking the presence of additional species or deviations from GR, either in the early or late Universe, see, e.g., [35–37]. However, without a complete observational picture from recombination to the present day, none of these proposed models is able to offer a satisfactory explanation. A novel and promising experimental probe is Line Intensity Mapping (LIM) (see e.g., [38] for a review, and references therein). LIM measures the integrated line emission of atomic or molecular spectral lines originating from unresolved sources, and, depending on the chosen spectral line, allows to bridge the gap between low- and high-redshift cosmological observables. Given the large number of LIM experiments that are taking and

will take place in the near future, see, e.g., refs. [39, 40], it is timely to investigate LIM potential to test the growth of structures.

Although several authors have already explored the possibility of using LIM to test deviations from Λ CDM at redshift $z \lesssim 6$ [41–46], the technique appears promising even for studying the reionization and cosmic dawn epochs [47]. However, in this work, we focus on the Hydrogen 21-cm line, which provides a rather unique access to the so-called “Dark Ages”, in the $30 \lesssim z \lesssim 200$ redshift window [48, 49]. The study of the Dark Ages is motivated by the presence of three significant features which make them the perfect target for high-precision cosmological measurements [50]: observables in this epoch *(i)* are well described by linear theory, *(ii)* provide access to a number of modes significantly larger than CMB experiments [51] since Hydrogen perturbations are not affected by Silk damping after photon-baryon decoupling, and *(iii)* suffer from minimal astrophysical uncertainties since stars have not formed yet.

In this work we showcase the outstanding potential of 21-cm LIM in constraining the growth of cosmic structure during the Dark Ages, thus in bridging the gap between recombination and the late Universe. Hereafter, the term “growth of structure” indicates the growth of matter density fluctuations in the linear regime, representing the first stage of cosmic web formation. We focus on both model-independent and model-dependent deviations from Λ CDM, where in the latter case we consider theoretical models of particular interest for early and late Universe phenomenology, such as Early Dark Energy [52, 53] and Dvali-Gabadadze-Porrati [54] models, respectively. These models differ from those investigated in ref. [55], where the deviations are induced by early Universe physics, at the level of the primordial curvature power spectrum. By contrasting Earth- and Moon-based experiments, we highlight the advantages of the latter in providing tighter constraints on the cosmological parameters associated to deviations from Λ CDM, with improvements ranging from a factor few to an order of magnitude. Moreover, if foregrounds are robustly accounted for, lunar experiments are able to reach percent and sub-percent precision on most models considered in this work, i.e., a precision competitive with that reached by complementary current and future cosmological experiments.

This article is organized as follows. In section 2 we review the theoretical basis of 21-cm LIM and useful statistical forecasting tools. In section 3 we describe alternative models that generate deviations from the Λ CDM growth of structure, while in section 4 we present the constraints on such models for future experiments. Finally, we conclude in section 5. Appendix A reviews the derivation of the angular power spectrum of 21-cm brightness temperature fluctuations, appendix B contains a discussion about how to account for the foreground wedge in harmonic space, while appendix C reports constraints corresponding to the figures presented in section 4.

2 Observing the Dark Ages

2.1 Hydrogen 21-cm line

The 21-cm Hydrogen spectral line corresponds to the hyperfine splitting of the ground state of neutral hydrogen into a singlet and triplet state [56–59]. The energy difference between the two states is $E_{21} = 5.9 \times 10^{-6}$ eV, thus the emitted photon has a wavelength of $\lambda_{21} = 21$ cm or, equivalently, a frequency of $\nu_{21} = 1420$ MHz. The relative occupation number density of neutral hydrogen atoms in the triplet (n_1) and singlet (n_0) states is encoded into the spin temperature T_s as

$$\frac{n_1}{n_0} = 3e^{-T_*/T_s}, \quad (2.1)$$

where $T_* = E_{21}/k_B = 68$ mK, and k_B is the Boltzmann constant. The spin temperature is determined by competing collisional and radiative processes. Collisions with free electrons, protons and neutral hydrogen atoms drive the spin temperature towards the Hydrogen kinetic temperature T_k , while absorption of and stimulated emission induced by CMB photons drive T_s towards the CMB temperature T_γ . Therefore, we can describe the spin temperature as a weighted average of kinetic and CMB temperatures as [48]

$$T_s^{-1} = \frac{T_\gamma^{-1} + x_k T_k^{-1}}{1 + x_k}, \quad x_k = \frac{T_*}{T_\gamma} \frac{C_{10}}{A_{10}}, \quad (2.2)$$

where C_{10} is the total collisional de-excitation rate [60], and A_{10} is the spontaneous emission coefficient of the 21-cm transition. Since the spin temperature is not directly observable, we aim to measure the 21-cm brightness temperature of neutral hydrogen in contrast with a background radio source (the CMB), which reads as

$$T_{21} = \frac{T_s - T_\gamma}{(1+z)}(1 - e^{-\tau_{21}}) \simeq \frac{T_s - T_\gamma}{(1+z)}\tau_{21}, \quad (2.3)$$

where the optical depth of the 21-cm line is given by

$$\tau_{21} = \frac{3x_{\text{HI}}n_H\lambda_{21}^3}{32\pi} \frac{E_{21}}{k_B T_s} \frac{A_{10}}{H(z) + (1+z)\partial_{\parallel}v_{\parallel}} \ll 1, \quad (2.4)$$

and x_{HI} is the neutral Hydrogen fraction, n_H is the Hydrogen number density, $H(z)$ is the Hubble expansion rate, and $\partial_{\parallel}v_{\parallel}$ is the comoving gradient of the gas velocity along the line of sight. During the Dark Ages, T_{21} departs from zero around redshift $z \sim 200$, when baryons thermally decouple from CMB photons and start cooling adiabatically, lowering the spin temperature to $T_s \simeq T_k < T_\gamma$. Therefore, the 21-cm signal is observed in absorption, i.e., $T_{21} < 0$.

In this work we focus on the statistics of 21-cm brightness temperature fluctuations around the global time-dependent background value \bar{T}_{21} , specifically on their two-point function in harmonic space. First we divide the total observational frequency band $\Delta\nu_{\text{tot}}$ into N_ν frequency bins of width $\Delta\nu$ centered at the observed frequency $\nu_i = \nu_{21}/(1+z_i)$, where z_i is the photon emission redshift. The angular power spectrum of the 21-cm brightness temperature fluctuations during the Dark Ages is well approximated by [61–63]

$$C_\ell^{ij} = 4\pi \int d\log k \mathcal{P}_\zeta(k) \mathcal{T}_\ell^{21}(k, \nu_i) \mathcal{T}_\ell^{21}(k, \nu_j), \quad (2.5)$$

where (i, j) label two arbitrary frequency channels, k 's are Fourier modes, and \mathcal{P}_ζ is the almost scale-invariant primordial curvature power spectrum. The 21-cm harmonic transfer function reads as

$$\mathcal{T}_\ell^{21}(k, \nu_i) = \int dr W_{\nu_i}(r) [\alpha(r) j_\ell(kr) - f(r) \bar{T}_{21}(r) \partial_{kr}^2 j_\ell(kr)] \mathcal{T}_b(k, r), \quad (2.6)$$

where r is the comoving distance, j_ℓ and $\partial_{kr}^2 j_\ell$ are Bessel functions and their second derivatives, respectively, $\alpha(r)$ is a time-dependent fitting function, $f(r) = d\log\delta_m/d\log a$ is the linear growth rate of matter density perturbations, $\mathcal{T}_b(k, r)$ is the baryon transfer function, and W_{ν_i} is a Gaussian window function centered at $r_i = r(z_i)$ with variance σ_i set by the frequency bin width as

$$\sigma_i = \frac{c(1+z_i)^2}{\nu_{21}H(z_i)} \frac{\Delta\nu}{2}, \quad (2.7)$$

where c is the speed of light. This choice of comoving distance bin width ensures that frequency cross-bin angular power spectra are negligible because the signal is dominated by purely local effects [62, 64]. The interested reader will find more details on the derivation of equation (2.5) in appendix A.

2.2 Forecasting the sensitivity of 21-cm experiments

The Fisher matrix analysis represents a convenient tool to forecast the precision of a hypothetical future experiment because it returns the best achievable error, i.e., the Cramér-Rao bound [65–68]. Under the assumption of Gaussian-distributed data, absence of coupling between multipoles, and absence of correlation between frequency bins, the exact Fisher matrix element [69] corresponding to the pair of cosmological parameters $\{\theta_\alpha, \theta_\beta\}$ reduces to

$$F_{\alpha\beta} = f_{\text{sky}} \sum_{i=1}^{N_\nu} \sum_{\ell=2}^{\ell_{i,\text{max}}} \sigma_{C_\ell^{ii}}^{-2} \frac{\partial C_\ell^{ii}}{\partial \theta_\alpha} \frac{\partial C_\ell^{ii}}{\partial \theta_\beta}, \quad (2.8)$$

where the parameter f_{sky} accounts for a partial coverage of the sky, the frequency-dependent multipole $\ell_{i,\text{max}}$ defines the maximum resolution of the experiment in a given frequency channel, and the angular power spectra covariance reads as

$$\sigma_{C_\ell^{ii}}^2 = \frac{2}{2\ell + 1} (C_\ell^{ii} + N_{i,\ell})^2, \quad (2.9)$$

where $N_{i,\ell}$ is the angular power spectrum of the noise in the i -th frequency channel. In the case of radio interferometers with uniformly distributed antennas, the noise angular power spectrum can be estimated as [49]

$$N_{i,\ell} = \frac{(2\pi)^3}{t_{\text{obs}}\Delta\nu} \left(\frac{T_{i,\text{sys}}}{f_{\text{cover}}\ell_{i,\text{max}}} \right)^2, \quad (2.10)$$

where t_{obs} is the total observation time, f_{cover} is the fraction of interferometer area covered with antennas, and $T_{i,\text{sys}}$ is the system temperature. The system temperature is dominated by galactic synchrotron radiation in every frequency channel of interest, thus we can approximate it as [56]

$$T_{i,\text{sys}} \approx 180 \left(\frac{\nu_i}{180 \text{ MHz}} \right)^{-2.6} \text{ K}, \quad (2.11)$$

where both the amplitude and the spectral index are compatible with recent EDGES measurements [70].¹ The maximum observable multipole is

$$\ell_{i,\text{max}} = \frac{2\pi D_{\text{base}}}{\lambda_i}, \quad (2.12)$$

where D_{base} is the largest baseline of the interferometer, and $\lambda_i = \lambda_{21}(1 + z_i)$ is the redshifted 21-cm wavelength. Finally, in order to understand the advantages of the tomographic approach, it is convenient to define a cumulative Fisher matrix as

$$F_{\alpha\beta}^{(N)} = f_{\text{sky}} \sum_{i=1}^N \sum_{\ell=2}^{\ell_{i,\text{max}}} \sigma_{C_\ell^{ii}}^{-2} \frac{\partial C_\ell^{ii}}{\partial \theta_\alpha} \frac{\partial C_\ell^{ii}}{\partial \theta_\beta}, \quad (2.13)$$

where we consider the contribution only of the first $N < N_\nu$ frequency channels. When $N = N_\nu$ we recover the Fisher matrix element of equation (2.8).

The cosmological parameters we consider in this work are divided into two broad classes, $\theta_{\Lambda\text{CDM}}$ and θ_{growth} , where the former contains the common core ΛCDM parameters while the latter contains the case-dependent parameters responsible for a growth of structure that deviates from ΛCDM , see section 3. Explicitly, the ΛCDM parameters considered in this work are

$$\theta_{\Lambda\text{CDM}} = \{100\theta_s, \omega_{\text{cdm}}, \omega_{\text{b}}, \log(10^{10}A_s), n_s\}, \quad (2.14)$$

where θ_s is the angular size of the sound horizon at recombination, ω_{cdm} and ω_{b} are the cold dark matter and baryon physical densities, respectively, A_s and n_s are the amplitude and tilt of the almost scale-invariant primordial curvature perturbation power spectrum, respectively. Ultimately, the errors on each cosmological parameter θ_α are provided by the diagonal elements of the inverse Fisher matrix defined in equation (2.8) as $\sigma_{\theta_\alpha} = \sqrt{(F^{-1})_{\alpha\alpha}}$. Similarly, the error coming from the cumulative Fisher approach in equation (2.13) is given by $\sigma_{\theta_\alpha}^{(N)} = \sqrt{((F^{(N)})^{-1})_{\alpha\alpha}}$. Therefore it is convenient to introduce the cumulative error ratio

$$\mathcal{C}_{\theta_\alpha} = \frac{\sigma_{\theta_\alpha}^{(N)}}{\sigma_{\theta_\alpha}}, \quad (2.15)$$

which quantifies how quickly we saturate the error obtained including all frequency bins, i.e., whether the additional frequency channels included in the analysis are noise- or signal-dominated.

¹This sky temperature is representative of observations performed at night, in a patch of sky that did not include the galactic center. Measurements of sky temperature of different patches or performed at different times return a larger value, see, e.g., refs. [70, 71], therefore the observation time does not necessarily reflect the “human” time.

Foregrounds represent a significant challenge for 21-cm cosmology, since they are 10^5 times larger than the signal we aim to constrain [72]. While synchrotron emission represents the main foreground, there are other (subdominant) foregrounds sourced for instance by free-free emission or galactic/extragalactic radio sources, that still dominate over the 21-cm signal. While in theory these smooth foregrounds can be subtracted from sky maps [73–75], the presence of instrumental systematics considerably limits this option, see, e.g., refs. [76–78]. Moreover, the presence of the ionosphere and radio frequency interference severely limits the exploitation of low frequency channels for an Earth-based experiment [79–82], thus the idea of designing a Moon-based observatory [83].

In this work we exploit the fact that many of these foregrounds, including those generated by the Earth’s atmosphere, appear to be comparable with thermal noise only in the so-called “foreground wedge” [84–93]. The foreground wedge is a section of the (k_\perp, k_\parallel) 2D Fourier space defined in each frequency channel by

$$k_\parallel \lesssim \theta_0 d_A(z_i) H(z_i) k_\perp, \quad (2.16)$$

where k_\parallel and k_\perp are the vectors parallel and across the line-of-sight, respectively, θ_0 is the field-of-view angle, and d_A is the angular diameter distance. Since the two-point function in harmonic space receives contributions from all k modes, we limit our analysis to those multipoles where contamination from foregrounds is kept at a reasonable minimum. Inspired by ref. [94], we consider both a “conservative” and “optimistic” scenario with respect to the perspective of foreground removal. In the former we consider contamination from systematics to be significant across the entire sky, i.e., $\theta_0^{\text{cons}} = \pi$, while in the latter we assume them to be restrained to the primary beam, i.e., $\theta_0^{\text{opt}} = 0.2$ [95, 96]. In terms of maximum multipoles, we have that the conservative and optimistic scenarios correspond to

$$\ell_{i,\text{for}}^{\text{cons}} \lesssim 0.14 \frac{\nu_i}{\delta\nu}, \quad \ell_{i,\text{for}}^{\text{opt}} \lesssim 2.24 \frac{\nu_i}{\delta\nu}, \quad (2.17)$$

respectively, where $\delta\nu$ is the spectral resolution of the measurement. We refer the reader to appendix B for the derivation of equation (2.17).

At the practical level, we consider four different experimental setups, including one state-of-the-art Earth-based experiment and three futuristic Moon-based observatories [97, 98].

- **aSKAO**, an advanced version of the Square Kilometer Array Observatory able to probe the end of the Dark Ages at redshift $z \approx 30$. This observatory has $N_\nu = 6$ frequency channels $\Delta\nu_{\text{tot}} = [40.3, 46.3]$ MHz with a bandwidth of $\Delta\nu = 1$ MHz, a baseline of $D_{\text{base}} = 100$ km, a cover fraction of $f_{\text{cover}} = 0.2$, and it observes the entirety of the sky, i.e., $f_{\text{sky}} = 0.75$, for $t_{\text{obs}} = 5$ yr.
- **LRA1**, a Lunar Radio Array on the far side of the Moon. It has the same bandwidth, fraction of observed sky, and observation time as aSKAO, but it has a baseline of $D_{\text{base}} = 30$ km, a cover fraction of $f_{\text{cover}} = 0.1$, and it observes the totality of the Dark Ages by having $N_\nu = 40$ frequency channels in the $\Delta\nu_{\text{tot}} = [6.3, 46.3]$ MHz frequency band.
- **LRA2**, a second, less conservative experiment, having the same specifics of LRA1 but with a baseline of $D_{\text{base}} = 100$ km and a cover fraction of $f_{\text{cover}} = 0.2$, as aSKAO.
- **LRA3**, a third Lunar Radio Array representing the ideal Moon-based interferometer. We extend the baseline to $D_{\text{base}} = 300$ km and increase the cover fraction to $f_{\text{cover}} = 0.75$.

The indicative resolution of the experiments is of order $\ell_{\text{max}}(z = 30) \simeq \mathcal{O}(10^5)$ and $\ell_{\text{max}}(z = 200) \simeq \mathcal{O}(10^4)$ for $D_{\text{base}} \sim 10^2$ km, decreasing by one order of magnitude for $D_{\text{base}} \sim 10$ km. Regarding the foreground wedge, we assume a spectral resolution of $\delta\nu = 10$ kHz [72, 99, 100]. Therefore, since $\ell_{i,\text{for}}^{\text{cons}} \simeq \mathcal{O}(10^2)$, we find that, in the conservative foreground removal scenario, excluding the foreground wedge from our analysis imposes a maximum multipole orders of magnitude smaller than that associated with the interferometer resolution. Instead, in the optimistic case, a smaller range of modes is lost to foreground removal since $\ell_{i,\text{for}}^{\text{opt}} \simeq \mathcal{O}(10^4)$. This resolution limitation highlights the need for developing efficient foreground-removal techniques to exploit the full potential of 21-cm Line Intensity Mapping.

3 Alternative models of structure growth

Since nonlinear effects and uncertainties connected to stellar evolution do not affect the 21-cm signal in the Dark Ages, we can use it as a “clean” probe of structure formation. We aim to test the capabilities of both Earth- and Moon-based experiments in constraining deviations from pure Λ CDM+GR, using both a model-dependent and -independent approach. All models considered in this work reproduce the Λ CDM background evolution history and have the same inflationary initial conditions. Deviations arise only at the level of growth of perturbations, either because of a modification of General Relativity or due to the presence of additional species. Some of the scenarios investigate deviations from Λ CDM happening during the Dark Ages themselves; others introduce new effects mainly during recombination or the post-reionization era, while still leaving a clear imprint also on the 21-cm signal. Remarkably, 21-cm experiments are sensitive enough to constrain also the latter classes of models. In all cases presented in this section, we employ modified versions of the public Boltzmann solver code **CLASS** [101] to compute the baryon transfer function, the growth rate, and other relevant quantities entering into the calculation of the angular power spectra defined in equation (2.5).

3.1 Model-independent approach on reconstructing growth history

Matter density perturbations δ_m grow at a rate proportional to the scale factor a at all scales during the matter-dominated era. Therefore, it is convenient to describe the growth of perturbation in terms of the linear growth rate function $f = d \log \delta_m / d \log a$. Following the approach of ref. [102], we model the growth rate as a step function which takes values $f_i = f(z_i)$ in each frequency channel. Each f_i is treated as an independent parameter in the forecast, thus in this case $\theta_{\text{growth}} = \{f_1, \dots, f_{N_\nu}\}$, with fiducial values taken from the publicly available code **CLASS** [101]. The fiducial values of the core Λ CDM parameters are taken from the *Planck* 2018 (TT,TE,EE + low-E) analysis and they read as [6]

$$\theta_{\Lambda\text{CDM}} = \{100\theta_s = 1.04109, \omega_{\text{cdm}} = 0.1202, \omega_b = 0.02236, \log(10^{10} A_s) = 3.045, n_s = 0.9649\}. \quad (3.1)$$

3.2 Deviations arising during the Dark Ages

Although many different General Relativity extensions have been explored during the past decades, see, e.g., ref. [103, 104] and refs. therein, here we implement an approach based on the “ $\mu - \eta$ ” parametrization [105, 106]. In this framework, the growth of structure at the linear level is altered by introducing two free functions of time and scale, $\mu(k, z)$ and $\eta(k, z)$, that effectively change the value of Newton’s constant G and the relation between the Bardeen potentials Ψ and Φ as

$$k^2 \Psi(k, z) = -4\pi G a^2 \mu(k, z) \bar{\rho} \Delta, \quad \Phi(k, z) = \eta(k, z) \Psi(k, z), \quad (3.2)$$

where $\bar{\rho}$ is the background energy density, and Δ is the gauge-invariant energy density contrast. In this work we consider

$$\mu(k, z) = 1 + (\mu_0 - 1) \mathcal{S}(k, z), \quad \eta(k, z) = 1 + (\eta_0 - 1) \mathcal{S}(k, z), \quad (3.3)$$

where the Λ CDM limit is recovered at all scales and redshifts when $\mu_0 = \eta_0 = 1$. The “switch” function \mathcal{S} is chosen in such a way that before and after the Dark Ages, and at small scales, we recover the Λ CDM limit even when $\mu_0, \eta_0 \neq 1$. Inspired by refs. [106–109], we define

$$\mathcal{S}(k, z) = \frac{1}{4} \left[1 - \tanh \left(\frac{z - z_{\text{on}}}{\Delta z_{\text{on}}} \right) \right] \left[1 - \tanh \left(\frac{z_{\text{off}} - z}{\Delta z_{\text{off}}} \right) \right] e^{-\frac{1}{2} (k/k_*)^2}, \quad (3.4)$$

where $z_{\text{on}}, z_{\text{off}}$ are two transition redshifts at which deviations are switched on and off, $\Delta z_{\text{on}}, \Delta z_{\text{off}}$ describe how fast the transition between the two regimes happens, and k_* is a reference scale above which deviations are gradually switched off. This scale dependence is inspired by, but not necessarily connected to, screening scenarios in Modified Gravity models [110–116]. When $z_{\text{off}} \lesssim z \lesssim z_{\text{on}}$ and $k \lesssim k_*$ we have $\mathcal{S}(k, z) \simeq 1$, thus $\mu \simeq \mu_0$ and $\eta \simeq \eta_0$, while in the opposite regimes $\mathcal{S}(k, z) \simeq 0$ and we recover the General Relativity limit.

We set $z_{\text{on}} = 500$, $z_{\text{off}} = 20$ and $\Delta z_{\text{on}} = 50$, $\Delta z_{\text{off}} = 4$ as reference values for the transition redshifts and widths, respectively. Regarding the reference scale, we choose $k_* = 10^{-2}, 10^{-1}, 1 \text{ Mpc}^{-1}$, as well as a scale-independent case where $k_* \rightarrow \infty$. The fiducial values for the core cosmological parameters are those of equation (3.1), while the fiducial values for the growth parameters are $\theta_{\text{growth}} = \{\mu_0 = 1, \eta_0 = 1\}$.

3.3 Late universe phenomenology

In this section we showcase the potential of 21-cm observations to constrain models that induce the bulk of their deviations from ΛCDM after the Dark Ages ended. One example of this class of theories is the Dvali-Gabadadze-Porrati (DGP) model [54], where deviations from General Relativity are a consequence of the propagation of gravity across an extra fifth dimension. The weakness of gravity is due to its propagation in a 5D Minkowski space, while our Universe remains embedded in 4D brane, i.e., the known 4D gravitational interaction is recovered only at short distances on the 4D brane. This theory has two branches of homogeneous and isotropic solutions, denoted as “normal” and “self-accelerating”. Here we focus on the normal branch of the theory (nDGP), since the self-accelerating branch is plagued by ghost instabilities [117, 118]. This class of models is a 1-parameter extension of ΛCDM , where the extra parameter is the crossover scale r_c between the 5D and 4D phenomenology of the theory.

In this work we consider the nDGP model proposed in ref. [119], where the ΛCDM expansion history is left unchanged but the growth of cosmic structure is altered. Growth of perturbations in nDGP can be conveniently remapped into the $\mu - \eta$ parametrization defined in equation (3.2) as [118, 120]

$$\mu(z) = 1 + \frac{1}{3\beta(z)}, \quad \eta(z) = \frac{1 - \frac{1}{3\beta(z)}}{1 + \frac{1}{3\beta(z)}}, \quad \beta(z) = 1 + \frac{H}{H_0\sqrt{\Omega_{\text{rc}}}} \left(1 + \frac{\dot{H}}{3H^2}\right), \quad (3.5)$$

where H_0 is the Hubble expansion rate today, \dot{H} is the Hubble expansion rate derivative with respect to cosmic time, and the parameter $\Omega_{\text{rc}}^{-1} = 4r_c^2 H_0^2$ quantifies the size of the crossover scale compared to that of the Hubble horizon today. When the crossover scale is much larger than the cosmological horizon, i.e., when $r_c H(z) \gg 1$, we have $\beta \rightarrow \infty$, thus $\mu, \eta \rightarrow 1$ and deviations from General Relativity are relegated to scales that cannot be probed by cosmological experiments. Even though during the Dark Ages nDGP models are responsible for a percent-level difference in the growth factor with respect to ΛCDM , these small deviations can still be captured by future 21-cm observations. Also in this case we consider as fiducial values for the cosmological parameters those appearing in equation (3.1), while we take $\theta_{\text{growth}} = \{\Omega_{\text{rc}} = 0.2\}$ as fiducial value for the extra nDGP parameter, motivated by current upper bounds [121].

3.4 Deviations arising before the Dark Ages

Finally, we also consider Early Dark Energy (EDE) models, which change the growth of structure before the beginning of the Dark Ages, leaving, however, a potentially detectable imprint in the 21-cm signal. EDE has been largely studied as a possible solution to the Hubble tension [122–126], since it induces a decrease in the size of the comoving sound horizon around recombination by increasing the Hubble expansion rate. Its phenomenology can be explained by the presence of an additional fluid with relative abundance of order 10% around matter-radiation equality, and equation of state such that $w_{\text{EDE}}(z \gtrsim 3300) \simeq -1$ and $w_{\text{EDE}}(z \lesssim 3300) \gtrsim 1/3$. In general, EDE models require a dark matter abundance larger than the ΛCDM one to avoid the decay of gravitational potentials around the time of recombination, the so-called “early ISW” effect, thus the growth of perturbations is naturally enhanced in this class of models [52].

A typical realization of EDE is achieved via an ultra-light self-interacting scalar field frozen in place by Hubble friction before recombination. Well-known candidates that display this phenomenology are axion-like particles [127–129] with potential

$$V(\phi_a) = m_a^2 f_a^2 \left(1 - \cos \frac{\phi_a}{f_a}\right)^n, \quad (3.6)$$

where the scalar field ϕ_a has mass $m_a \sim 10^{-27}$ eV, f_a is a characteristic energy scale, and we consider $n = 3$ to avoid additional fine tuning of the potential [130]. This choice of the exponent also agrees with the most likely value found by Cosmic Microwave Background, Baryon Acoustic Oscillations and Supernovae data joint-analysis [52]. Instead of directly working with parameters appearing in the Lagrangian, it is convenient to use the alternative set of parameters $\{f_{\text{EDE}}, \log_{10} z_c, \theta_{\text{ini}}\}$, where f_{EDE} is the ratio between EDE density and the critical one evaluated at critical redshift z_c , at which EDE becomes dynamical, and $\theta_{\text{ini}} = \phi_{a,\text{ini}}/f_a$ is the normalized scalar field initial value. We use CLASS-EDE [130], a publicly available modified version of CLASS, to estimate EDE effects on matter power spectra. In this case, fiducial values for the cosmological and growth parameters are $\theta_{\Lambda\text{CDM}} = \{100\theta_s = 1.04152, \omega_{\text{cdm}} = 0.1306, \omega_b = 0.02253, \log(10^{10} A_s) = 3.098, n_s = 0.9889\}$ and $\theta_{\text{growth}} = \{f_{\text{EDE}} = 0.122, \log_{10} z_c = 3.562, \theta_{\text{ini}} = 2.83\}$, respectively [125].

4 Constraints on the growth of structure

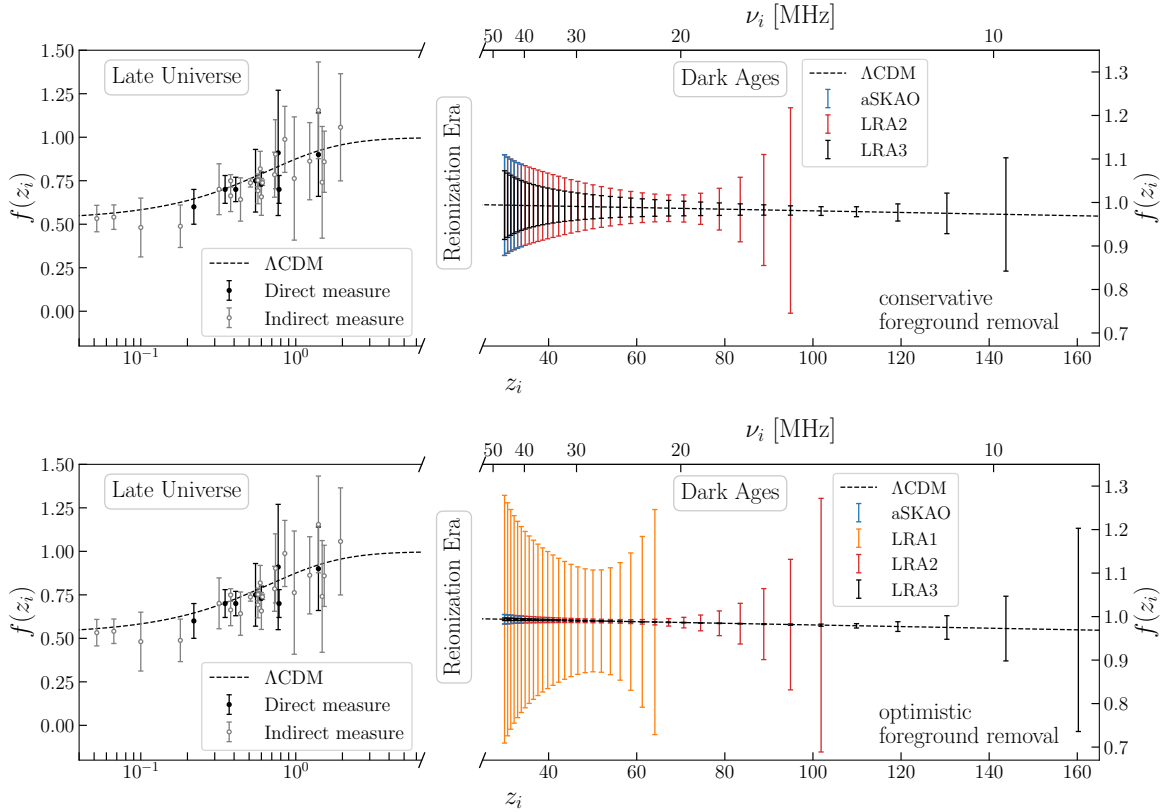


Figure 1: Direct (*black*) and indirect (*gray*) measures of the growth rate in the late Universe [9–27], ΛCDM theoretical values (*black dashed line*), and predicted sensitivity for individual frequency channels of aSKAO (*blue*), LRA1 (*orange*) LRA2 (*red*) and LRA3 (*black*) with conservative (*top panel*) and optimistic (*lower panel*) foreground removal. In the case of Dark Ages experiments we report constraints only for those frequency channels where a precision of order 30% is reached. For the sake of clarity, note that the left and right y-axis scales do not match.

Galaxy redshift surveys provide a large number of independent measurements of the growth history at redshift $z \lesssim 2$ by targeting different kinds of tracers (LRG, ELG, Ly α , voids, etc.) [9–27]. These growth rate measurements are either “direct” or “indirect”, where the former means that individual $f(z_i)$ s are estimated from data, while in the latter case the measured quantity is $f(z)\sigma_8(z)$, where $\sigma_8(z) = D(z)\sigma_8$, $D(z)$ is the linear growth factor normalized to unity at redshift $z = 0$, and σ_8

is the linear matter field fluctuation RMS today, see, e.g., ref. [29, 131] for an overview. Similarly, measuring the 21-cm line at different frequencies allows to investigate structure formation over a wide range of redshifts and reconstruct the neutral hydrogen distribution via a tomographic analysis.

We show in figure 1 the present and expected (at the moment of this work) future landscape of $f(z)$ measurements. Late Universe indirect measurements are converted into growth rate estimates by imposing a Planck prior on σ_8 [6]. The high-redshift late Universe ($z \gtrsim 2$) is still an uncharted epoch, however future experiments such as SPHEREx[132–134], Roman [135], and the proposed MegaMapper [136, 137] and SIRMOS [138], will be able to explore even that redshift range. We were unable to find constraints on the growth rate during the reionization era, between redshift $6.5 \lesssim z \lesssim 30$, however we note that the Hydrogen 21-cm line signal is still present in that epoch, even though in that case it is also affected by star and galaxy formation processes [56, 57]. Finally, we present the forecast on the growth rate for our four experimental setups. We observe that, even in the conservative foreground removal scenario, lunar experiment configurations with a baseline of order $D_{\text{base}} \sim 10^2$, achieve a precision below the 10% level over a remarkably broad redshift range, namely $33 < z_i \lesssim 85$ and $30 < z_i \lesssim 130$ for LRA2 and LRA3, respectively. Outside these ranges, errors rapidly increase because synchrotron radiation noise dominates over the clustering signal at low frequencies, thus we do not display those results. As a consequence, in the optimistic foreground removal scenario, the aforementioned ranges extend only slightly to $30 < z_i \lesssim 90$ for LRA2 and $30 < z_i \lesssim 140$ for LRA3. However, in this case, sub-percent precision is achievable for $30 < z_i \lesssim 65$ (LRA2) and $30 < z_i \lesssim 110$ (LRA3). This sensitivity allows us to test even models that affect the growth of structure mostly outside of the Dark Ages. At last, the smaller baseline and cover fraction of LRA1 limit its constraining capability to 10 – 30% in the redshift range $30 < z \lesssim 65$ in the optimistic case, and to remain above the 45% level in the conservative one. Overall, we note that the maximum sensitivity is typically reached around frequencies probing $z_i \approx 50 - 60$, where the amplitude of the angular power spectrum of 21-cm fluctuations reaches its maximum.

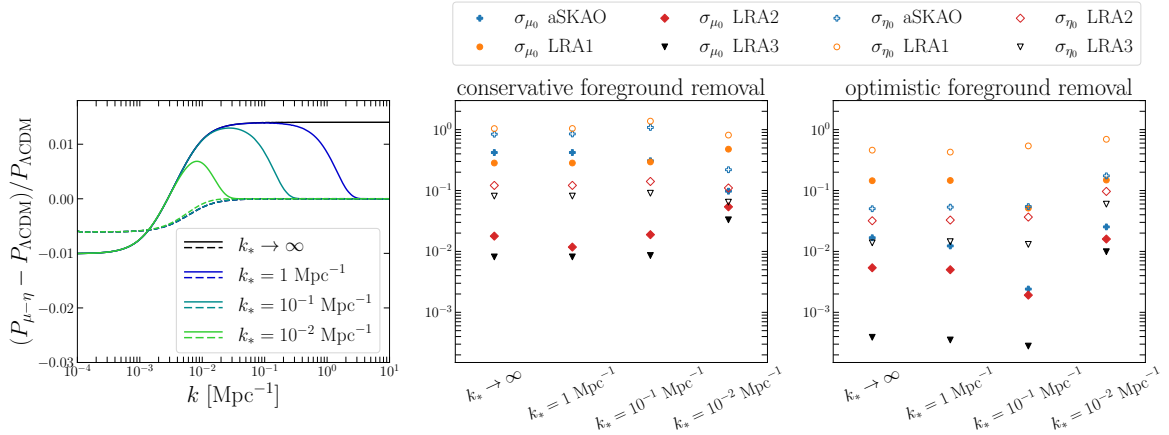


Figure 2: *Left panel:* $\mu - \eta$ matter power spectrum relative deviation with respect to $\Lambda\text{CDM} + \text{GR}$ prediction at redshift $z = 30$. Different scale-dependent deviations are induced by individual 0.5% changes from unity in the μ_0 (solid lines) or η_0 (dashed lines) parameters, while keeping the other ones fixed at their $\Lambda\text{CDM} + \text{GR}$ values. *Center and right panel:* marginalized errors on μ_0 (filled markers) and η_0 (empty markers) for aSKAO (blue), LRA1 (orange), LRA2 (red), and LRA3 (black) with conservative and optimistic foreground removal. The fiducial values of the parameters used for the Fisher forecast are $\{\mu_0 = 1, \eta_0 = 1\}$; ΛCDM parameters as listed in equation (3.1).

In terms of model-dependent deviations from ΛCDM during the Dark Ages, we show in the left panel of figure 2 the effects of changing the evolution of the Bardeen potentials on the matter power spectrum and, in the center and right panels, the constraints we find on the μ_0, η_0 parameters. The left panel reports the relative difference between the matter power spectrum when varying μ_0 or η_0 by 0.5% from unity for different choices of k_* . While μ alters in opposite fashions the growth of

structure at scales above and below the cosmological horizon $k_{\text{hor}} \simeq aH \approx 10^{-3} \text{ Mpc}^{-1}$, η induces appreciable changes only on super-horizon scales and on a restricted range of the largest sub-horizon scales, thus we expect constraints on this parameter to be less tight. The chosen values of k_* reflect those scales our experiments will be mostly sensitive to. Already at this point, we note that k_* choices in the η function have little to no impact in altering the matter power spectrum at redshift $z = 30$.

We observe in the center and right panels of figure 2 the benefits of a tomographic approach, especially with conservative foreground removal. In this case, Moon-based experiments yield constraints that are typically an order of magnitude tighter than those coming from the ground, when baselines are comparable. When comparing the optimistic and conservative foreground removal scenarios for a fixed instrumental configuration, in most instances of interest, errors increase by at least one order of magnitude for aSKAO but only by a factor of 3 or less for LRA configurations, highlighting how tomography makes constraints less sensitive to the amount of modes lost to the foreground wedge. Moreover, while constraints on μ_0 depend on the choice of k_* , constraints on η_0 do not, because it only affects the growth of the largest sub-horizon modes. Finally, when the growth of perturbations differs only on large scales, as in the $k_* = 10^{-2} \text{ Mpc}^{-1}$ case, constraints become less tight because of the $\mu_0 - \eta_0$ degeneracy due to the fact that they induce a similar scale-dependent suppression/enhancement on the matter power spectrum. We report in table 1 of appendix C the marginalized errors displayed in the center and right panels of figure 2. Additionally, we explicitly check that marginalized errors do not change by more than a factor of a few when varying the transition speeds $\Delta z_{\text{on}}, \Delta z_{\text{off}}$.

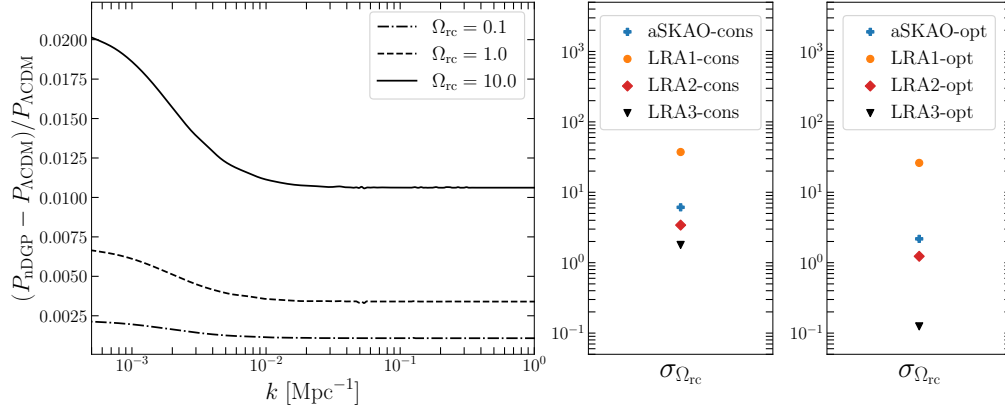


Figure 3: *Left panel:* nDGP matter power spectrum relative deviation with respect to Λ CDM prediction at redshift $z = 30$. *Center and right panel:* marginalized errors on Ω_{rc} for aSKAO (blue), LRA1 (orange), LRA2 (red) and LRA3 (black) with conservative and optimistic foreground removal. Fiducial values of the parameters used for the Fisher forecast: $\{\Omega_{\text{rc}} = 0.2\}$; Λ CDM parameters as listed in equation 3.1.

Thanks to their remarkable sensitivity, 21-cm Moon-based experiments also have the potential to provide a complementary test of theories that significantly differ from Λ CDM only at late times. The nDGP model induces deviations in the matter power spectrum at all scales, as can be seen in the left panel of figure 3. The scale-dependence is exclusively due to the fact that sub- and super-horizon modes grow at a different pace when $\{\mu, \eta\} \neq 1$, as we already illustrated in the previous scenario. We observe in the center and right panels of figure 3 that most experimental configurations examined in this work have no constraining power over Ω_{rc} , even when considering optimistic foreground removal. Only an experiment with instrumental specifics comparable to those of LRA3 is able to constrain Ω_{rc} down to the 60% precision level in the optimistic case and therefore provide competitive and complementary constraints on this class of theories with respect to existing [28, 121] and future [109, 139, 140] surveys. Also in this case we report in table 2 of appendix C the values of marginalized errors displayed in the center and right panels of figure 3. Moreover, we find that marginalized relative errors are largely unaffected by one order of magnitude changes in the fiducial value of Ω_{rc} .

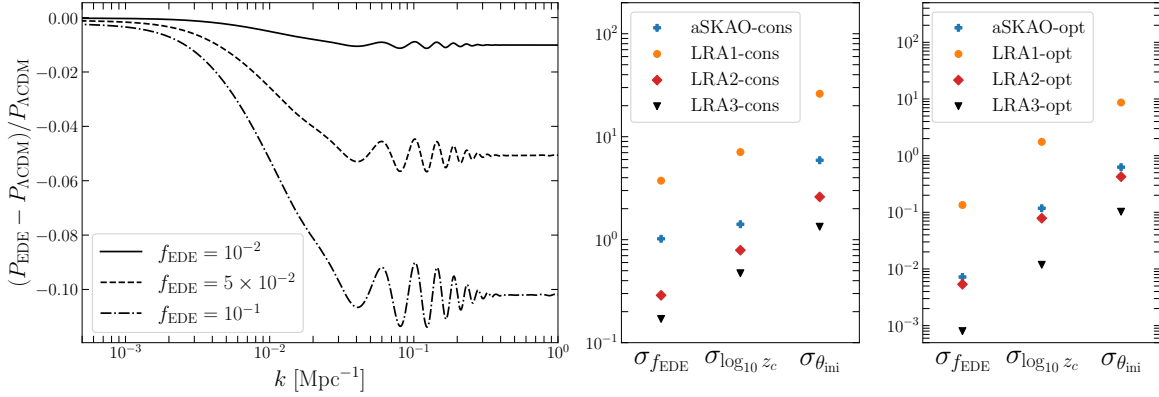


Figure 4: *Left panel:* EDE matter power spectrum relative deviation with respect to Λ CDM prediction at redshift $z = 30$ for different EDE abundance. Cosmological parameter for Λ CDM are given in equation (3.1). EDE fixed parameters are $\{\log_{10} z_c = 3.562, \theta_{\text{ini}} = 2.83\}$. *Center and right panel:* marginalized errors on EDE model parameters for aSKAO (blue), LRA1 (orange), LRA2 (red) and LRA3 (black) with conservative and optimistic foreground removal. Fiducial values of the parameters used for the Fisher forecast: $\{f_{\text{EDE}} = 0.122, \log_{10} z_c = 3.562, \theta_{\text{ini}} = 2.83\}$; Λ CDM parameters as listed in section 3.4.

Following a similar logic, we turn our attention to the Early Dark Energy (EDE) scenario, where deviations from Λ CDM take place considerably before the onset of the Dark Ages, around the time of matter-radiation equality. Because of the decay of gravitational potentials due to EDE, the growth of matter perturbations is suppressed when compared to Λ CDM. Thus, we expect such a model to leave an imprint that is potentially detectable even at lower redshift despite the EDE fluid itself decays away faster than radiation, as we show in the left panel of figure 4. In the conservative scenario, foreground removal highly limits the constraining capability on EDE parameters for all instrumental setups, since the majority of small scales where the growth is damped by EDE are removed with the wedge. In the optimistic scenario, aSKAO and LRA2 constraints on EDE parameters are compatible with existing constraints found by complementary datasets (*Planck* TT,TE,EE + lensing, BAO, Pantheon SNIa, SHOES), see, e.g., refs. [52, 125, 141]. Finally, we find that the LRA3 configuration can improve constraints on f_{EDE} and $\log_{10} z_c$ by at least an order of magnitude, and enhance the precision on θ_{ini} by a factor of a few. In particular, given that solving the Hubble tension requires an abundance of EDE of order $f_{\text{EDE}} \simeq 10^{-1}$, all examined configurations except LRA1 can detect the presence of EDE-induced effects (for such abundances) at more than 5σ level in the optimistic case, potentially providing a definitive answer regarding the viability of this candidate as a solution to the Hubble tension. As before, we report in table 3 of appendix C the values of marginalized errors displayed in the center and right panels of figure 3.

Finally, we analyze the gain in constraining power given by a tomographic approach. In particular, in figures 5 and 6 of appendix C we compare the marginalized error obtained by using only the first N frequency channels (and so redshift bins) with that obtained using all of them. Despite being severely limited by foregrounds, it appears that Earth-based experiment would still benefit from having a handful more frequency channels, even though this kind of consideration has to be validated by more accurate predictions of the effects of systematics. Conversely, we note that in LRA experiments, most of the information is contained in the first twenty channels, with marginal gains obtained by pushing tomography to even lower frequencies (higher redshifts), where thermal noise completely dominates the anisotropic clustering signal.

Constraints reported in this section are marginalized over the set of core cosmological parameters. We find that in the vast majority of cases marginalization does not affect the magnitude of New Physics parameters by more than a factor of a few, preserving the order of magnitude of the errors. Also, by the time these experiments start observations, the set of core cosmological parameters will already

be measured with a very high degree of precision and accuracy, effectively mimicking the effect of marginalization.

5 Conclusions

Detecting anisotropies in the 21-cm brightness temperature of neutral Hydrogen will allow to reconstruct not only its spatial distribution, but also to trace structure formation across a currently unexplored redshift range. In this work we investigated the potential of future Earth- and Moon-based 21-cm Line Intensity Mapping (LIM) surveys to constrain the growth of cosmic structures, both in a model -dependent and -independent fashion. In particular, we focused on the Dark Ages because of their complementarity with existing cosmological observations and their insensitivity to uncertainties related to the development of non-linear structures and astrophysical processes. We produce forecasts for both Earth-based surveys, which are able to reach only the end of the Dark Ages at $z \sim 30$, and for a futuristic Moon-based instrument that will observe the entirety of the Dark Ages and avoid foregrounds generated by the Earth’s atmosphere. There is not yet a consensus on the efficiency of foreground removal in the frequency range of interest; therefore, we present results for both a pessimistic scenario, employing a conservative foreground removal strategy, and an optimistic one that showcases the full potentialities of 21-cm LIM.

Our results show that Moon-based 21-cm LIM surveys with a baseline of order $\sim 10^2$ km reach at minimum a ten percent precision level on the growth rate measurements over an extended redshift range during the Dark Ages. The sensitivity of future 21-cm LIM surveys will enable high-precision constraints on theories that predict deviations from Λ CDM at different moments of cosmic history, during and even outside the Dark Ages themselves. In particular, we focus on the nDGP model, which introduces deviations from General Relativity mostly at low redshifts (even though its percent-level difference in the growth factor is still observable during the Dark Ages) in order to explain the accelerated expansion, and on the EDE model, which alleviates the Hubble tension by introducing a new component behaving like Dark Energy that becomes relevant before recombination. Even though most of the constraining power resides at lower redshifts, accessible also to Earth-based surveys, Moon-based experiments still provide tighter constraints, with precision improvements ranging from a factor of a few up to an order of magnitude. Lunar configurations, in fact, can take advantage of their higher redshift reach to mitigate the effect of the loss of modes due to foreground removal, and to break degeneracies between cosmological parameters. We showed that, under optimistic foreground removal, lunar experiments will provide constraints competitive with future galaxy surveys and gravitational waves datasets for nDGP models, and will either confirm or disprove at more than 5σ level the viability of EDE as a solution to the Hubble tension. The strength of these experiments does not reside only in their constraining power on cosmological parameters, but also in their complementarity with current and future observations since they will test an epoch of the Universe currently unexplored.

We explore how LIM measurements during the Dark Ages can help bridge the gap in understanding the growth of cosmic structure between the epoch of recombination and the late Universe. Future galaxy and LIM surveys have the potential to cover not only the redshift range corresponding to the high-redshift Universe, but also that corresponding to the epoch of reionization and cosmic dawn, providing unique insights on cosmology. We envision that cross-correlating signals coming from different epochs will provide very stringent tests on multiple beyond- Λ CDM models, and eventually it will either confirm or rule out several new physics candidates that are currently adopted to solve cosmological tensions. In conclusion, despite current technological limitations, future 21-cm LIM surveys will allow cosmology to enter a new era of precision measurements.

Acknowledgments

The authors would like to thank Andrea Begnoni, Jessie de Kruijf, Sarah Libanore, and Gabriele Perna for useful discussions. Elena Vanetti acknowledges partial financial support by ASI Grant No. 2016-24-H.0. The project that gave rise to these results received the support of a fellowship from the a “Caixa” Foundation (ID B006373). The fellowship code is LCF/BQ/DI24/12070001. Nicola

Bellomo is supported by PRD/ARPE 2022 “Cosmology with Gravitational waves and Large Scale Structure - CosmoGraLSS”. AR acknowledges funding from the Italian Ministry of University and Research (MUR) through the “Dipartimenti di eccellenza” project “Science of the Universe”.

A The angular power spectrum of 21-cm brightness temperature fluctuations

The purpose of this appendix is to keep track of some of the steps taken to derive equation (2.5). As recently pointed out in ref. [142], the finite width of the 21-cm line requires the definition of the spin temperature to be changed to

$$T_s^{-1} = \frac{x_{\text{CMB}} T_\gamma^{-1} + x_k T_k^{-1}}{x_{\text{CMB}} + x_k}, \quad (\text{A.1})$$

where $x_{\text{CMB}} = \tau_{21}^{-1} (1 - e^{-\tau_{21}})$. However, during the Dark Ages we are consistently in the optically-thin regime, since between redshift 30 and 200 we have $\tau_{21} \in [0.02, 0.05]$, approximately. Thus, the correction to the 21-cm brightness temperature induced by the finite width of the line is estimated to be of order $\mathcal{O}(\tau_{21}/2)$, i.e., $1 - 2.5\%$ [142]. Although precision measurements of the 21-cm temperature will require an equally careful estimation of the theoretical signal, we choose for the moment to neglect these percent effect because we are not in possession of an equally accurate knowledge of the expected level of noise.

Fluctuations in the 21-cm brightness temperature are commonly approximated as (see, e.g., appendix B of ref. [61])

$$\delta T_{21} \simeq f_H \delta_H + f_{T_k} \delta_{T_k} + \bar{T}_{21} \delta_v, \quad (\text{A.2})$$

where δ_H and δ_{T_k} are the neutral hydrogen number density and kinetic temperature, respectively, the velocity perturbation δ_v reads as

$$\delta_v = -\frac{1+z}{H(z)} \partial_{\parallel} v_{\parallel}, \quad (\text{A.3})$$

and f_H, f_{T_k} are time-dependent functions given, for instance, in appendix B of ref. [61]. We neglect fluctuations in the CMB temperature and ionization fraction in our derivation, since they have been shown to be subdominant in ref. [62].

In this work we follow the approach developed in ref. [63] to connect baryon temperature and velocity fluctuations to the baryon overdensity perturbation. Regarding the former, it was noted that under the approximation that baryons track dark matter evolution, thus $\delta_b \propto a$, it is possible to recast the temperature perturbation as $\delta_{T_k}(t) = C(t) \delta_b(t)$. The functional form of $C(t)$ is derived by solving the perturbed first law of thermodynamics

$$\dot{\delta}_{T_k} - \frac{2}{3} \dot{\delta}_b + \Gamma_C \frac{T_\gamma}{T_k} \delta_{T_k} = 0, \quad (\text{A.4})$$

with initial conditions $\delta_{T_k, \text{ini}} = 0$, where Γ_C is the Compton scattering rate, and dots indicate derivatives with respect to cosmic time. Moreover, on top of this analytical argument, we also numerically check with CLASS that such function C has a negligible scale dependence in the range of scales of interest for this work. On the other hand, the velocity perturbation can be recast in terms of the baryon overdensity fluctuation using the continuity equation $\dot{\delta}_b + a^{-1} \theta_b = 0$, where θ_b is the baryon velocity divergence, thus $\theta_b = -aH f_b \delta_b$, where f_b is the growth rate of baryon density fluctuations, defined as $f_b = d \log \delta_b / d \log a$. For the sake of facilitating a comparison with traditional large-scale structure growth rate measurements, we assume $f_b \simeq f$. In reality, especially at the beginning of the Dark Ages, f *underestimates* the real value of f_b , since baryons have not already caught up with dark matter, especially at small scales; thus, with our forecast we obtain *more conservative*, i.e., larger, errors. On the other hand, we verified that towards the end of the Dark Ages, where most of the constraining power of our experiments reside (see, e.g., figures 5 and 6), constraints on f are fundamentally unaffected by this assumption. Finally, since $\delta_H \sim \delta_b$, we arrive at the following expression in Fourier space

$$\delta T_{21}(\mathbf{k}, r(z)) = [\alpha(z) + \mu^2 f(z) \bar{T}_{21}(z)] \delta_b(\mathbf{k}, z), \quad (\text{A.5})$$

where $\alpha = f_H + C f_{T_k}$, and μ is the cosine of the angle between the Fourier mode \mathbf{k} and the line-of-sight \mathbf{r} . The spherical harmonic coefficients, as per common practice, are obtained as

$$a_{\ell m}^i = \int d\Omega_{\hat{\mathbf{r}}} Y_{\ell m}^*(\hat{\mathbf{r}}) \times \int dr W_{\nu_i}(r) \int \frac{d^3 k}{(2\pi)^3} e^{i\mathbf{k} \cdot \mathbf{r}} \delta T_{21}(\mathbf{k}, r). \quad (\text{A.6})$$

Equation (2.5) is then easily obtained by taking the expectation value of pairs of spherical harmonic coefficients, where derivatives of Bessel functions appear by recasting μ^2 in terms of derivatives of $e^{i\mathbf{k}\cdot\mathbf{r}}$.

The authors of ref. [62] correctly pointed out that the RHS of equation (A.2) should be multiplied by a common factor of $e^{-\tau_{\text{reio}}}$, where τ_{reio} is the reionization optical depth. Therefore, the angular power spectra of 21-cm brightness temperature is expected to be damped by a factor $e^{-2\tau_{\text{reio}}} \sim 0.9$, approximately, according to the latest Planck data release [6]. As for the effect of finite width of the 21-cm line, we expect that not including this effect will have a minimal impact on our results, especially in the case where the level of the noise is not known to a percent-level accuracy. If included, this effect would realistically increase the error bars by a few percent of their current values reported in appendix C, preserving the overall conclusions. Moreover, we expect this additional exponential damping of the signal to be extremely degenerate with the amplitude of primordial fluctuations, making it effectively equivalent to a constant rescaling of the latter.

B Angular resolution in presence of foregrounds

Radio interferometers observe modes within a cylindrical volume in Fourier space given by

$$V_k \simeq \pi (k_{\perp,\text{max}}^2 - k_{\perp,\text{min}}^2) (k_{\parallel,\text{max}} - k_{\parallel,\text{min}}), \quad (\text{B.1})$$

where $k_{\perp,\text{max}}$ and $k_{\perp,\text{min}}$ are determined by the field of view and the array of antennas, respectively, while $k_{\parallel,\text{max}}$ and $k_{\parallel,\text{min}}$ depend on the spectral resolution of the instrument and the bandwidth chosen for the analysis. In a full-sky survey we can safely approximate $k_{\perp,\text{min}} \simeq 0$, thus we neglect it in the following derivation. The volume occupied by the foreground wedge in each frequency channel, i.e., the region satisfying equation (2.16), is

$$V_{\text{wedge}} \simeq \frac{2}{3} \pi k_{\perp,\text{max}}^2 (k_{\text{wedge,max}} - k_{\parallel,\text{min}}), \quad (\text{B.2})$$

where

$$k_{\text{wedge,max}} = \theta_0 d_A(z_i) H(z_i) k_{\perp,\text{max}}, \quad (\text{B.3})$$

while the foreground-free volume reads as

$$V_{\text{ff}} = V_k - V_{\text{wedge}} \simeq \pi k_{\perp,\text{max}}^2 \left[k_{\parallel,\text{max}} - k_{\text{wedge,max}} + \frac{1}{3} (k_{\text{wedge,max}} - k_{\parallel,\text{min}}) \right]. \quad (\text{B.4})$$

We define a maximum resolution $\ell_{i,\text{for}}$ to minimize the impact of Fourier modes contaminated by foregrounds in the estimation of the angular power spectra. Specifically, we require that the volume of foreground-free modes dominates over the volume of the wedge, i.e., that $V_{\text{ff}} \gtrsim \alpha_V V_{\text{wedge}}$, where α_V is an arbitrary numerical coefficient. This requirement explicitly reads as

$$k_{\parallel,\text{max}} \gtrsim \frac{2\theta_0}{3} (\alpha_V + 1) d_A(z_i) H(z_i) k_{\perp,\text{max}}, \quad (\text{B.5})$$

or, in terms of multipole resolution, as

$$\ell_{i,\text{for}} \lesssim \frac{3\pi}{\theta_0(\alpha_V + 1)} \frac{\nu_i}{\delta\nu}, \quad (\text{B.6})$$

where we use $\ell_{i,\text{for}} \simeq k_{\perp,\text{max}} r_i$ and $k_{\parallel,\text{max}} \simeq 2\pi \frac{H(z_i)\nu_i}{(1+z_i)\delta\nu}$. In this work we assume the conservative value of $\alpha_V = 20$, i.e., only less than 5% of k modes are impacted by foregrounds, recovering equation (2.17).

C Tables of constraints and cumulative errors

In this appendix we report the numerical values of the constraints presented in the figures of section 4. Moreover, to highlight the constraining power obtained by including additional frequency channels to a given experiment, we show the cumulative error ratio defined in equation (2.15) in figures 5 and 6, for the conservative and optimistic foreground removal cases respectively.

Experiment	$k_* [\text{Mpc}^{-1}]$	conservative		optimistic	
		σ_{μ_0}	σ_{η_0}	σ_{μ_0}	σ_{η_0}
aSKAO	$\rightarrow \infty$	4.21×10^{-1}	8.41×10^{-1}	1.68×10^{-2}	5.02×10^{-2}
	1	4.21×10^{-1}	8.49×10^{-1}	1.23×10^{-2}	5.33×10^{-2}
	10^{-1}	3.08×10^{-1}	1.09	2.41×10^{-3}	5.45×10^{-2}
	10^{-2}	9.75×10^{-2}	2.20×10^{-1}	2.53×10^{-2}	1.74×10^{-1}
LRA1	$\rightarrow \infty$	2.83×10^{-1}	1.04	1.45×10^{-1}	4.60×10^{-1}
	1	2.83×10^{-1}	1.04	1.46×10^{-1}	4.28×10^{-1}
	10^{-1}	2.95×10^{-1}	1.38	5.14×10^{-2}	5.40×10^{-1}
	10^{-2}	4.78×10^{-1}	8.13×10^{-1}	1.49×10^{-1}	6.94×10^{-1}
LRA2	$\rightarrow \infty$	1.78×10^{-2}	1.21×10^{-1}	5.39×10^{-3}	3.19×10^{-2}
	1	1.18×10^{-2}	1.21×10^{-1}	5.01×10^{-3}	3.27×10^{-2}
	10^{-1}	1.88×10^{-2}	1.41×10^{-1}	1.92×10^{-3}	3.66×10^{-2}
	10^{-2}	5.39×10^{-2}	1.10×10^{-1}	1.60×10^{-2}	9.67×10^{-2}
LRA3	$\rightarrow \infty$	8.12×10^{-3}	8.10×10^{-2}	3.89×10^{-4}	1.38×10^{-2}
	1	8.13×10^{-3}	8.11×10^{-2}	3.51×10^{-4}	1.45×10^{-2}
	10^{-1}	8.57×10^{-3}	9.03×10^{-2}	2.79×10^{-4}	1.31×10^{-2}
	10^{-2}	3.30×10^{-2}	6.44×10^{-2}	9.89×10^{-3}	5.97×10^{-2}

Table 1: Marginalized errors on μ_0 and η_0 for aSKAO, LRA1, LRA2 and LRA3 in the conservative and optimistic case. For a visual comparison, we refer the reader to the central and right panel of figure 2. Fiducial values of the parameters used for the Fisher forecast: $\{\mu_0 = 1, \eta_0 = 1\}$; Λ CDM parameters as listed in equation (3.1)

Experiment	conservative	optimistic
	$\sigma_{\Omega_{\text{rc}}}$	$\sigma_{\Omega_{\text{rc}}}$
aSKAO	6.11	2.18
LRA1	37.32	26.13
LRA2	3.42	1.23
LRA3	1.79×10^{-1}	1.25×10^{-1}

Table 2: Marginalized errors on Ω_{rc} for aSKAO, LRA1, LRA2 and LRA3 in the conservative and optimistic case. For a visual comparison, we refer the reader to the central and right panels of figure 3. Fiducial values of the parameters used for the Fisher forecast: $\{\Omega_{\text{rc}} = 0.2\}$; Λ CDM parameters as listed in equation (3.1).

Experiment	conservative			optimistic		
	$\sigma_{f_{\text{EDE}}}$	$\sigma_{\log_{10} z_c}$	$\sigma_{\theta_{\text{ini}}}$	$\sigma_{f_{\text{EDE}}}$	$\sigma_{\log_{10} z_c}$	$\sigma_{\theta_{\text{ini}}}$
aSKAO	1.02	1.41	5.91	7.21×10^{-3}	1.18×10^{-1}	6.26×10^{-1}
LRA1	3.74	7.09	26.14	1.35×10^{-1}	1.75	8.65
LRA2	2.88×10^{-1}	7.90×10^{-1}	4.60	5.36×10^{-3}	7.86×10^{-2}	4.25×10^{-1}
LRA3	1.70×10^{-1}	4.72×10^{-1}	1.34	7.98×10^{-4}	1.18×10^{-2}	1.02×10^{-1}

Table 3: Marginalized errors on f_{EDE} , $\log_{10} z_c$ and θ_{ini} for aSKAO, LRA1, LRA2 and LRA3 in the conservative and optimistic case. For a visual comparison, we refer the reader to the central and right panels of figure 4. Fiducial values of the parameters used for the Fisher forecast: $\{f_{\text{EDE}} = 0.122, \log_{10} z_c = 3.562, \theta_{\text{ini}} = 2.83\}$; Λ CDM parameters as listed in section 3.4.

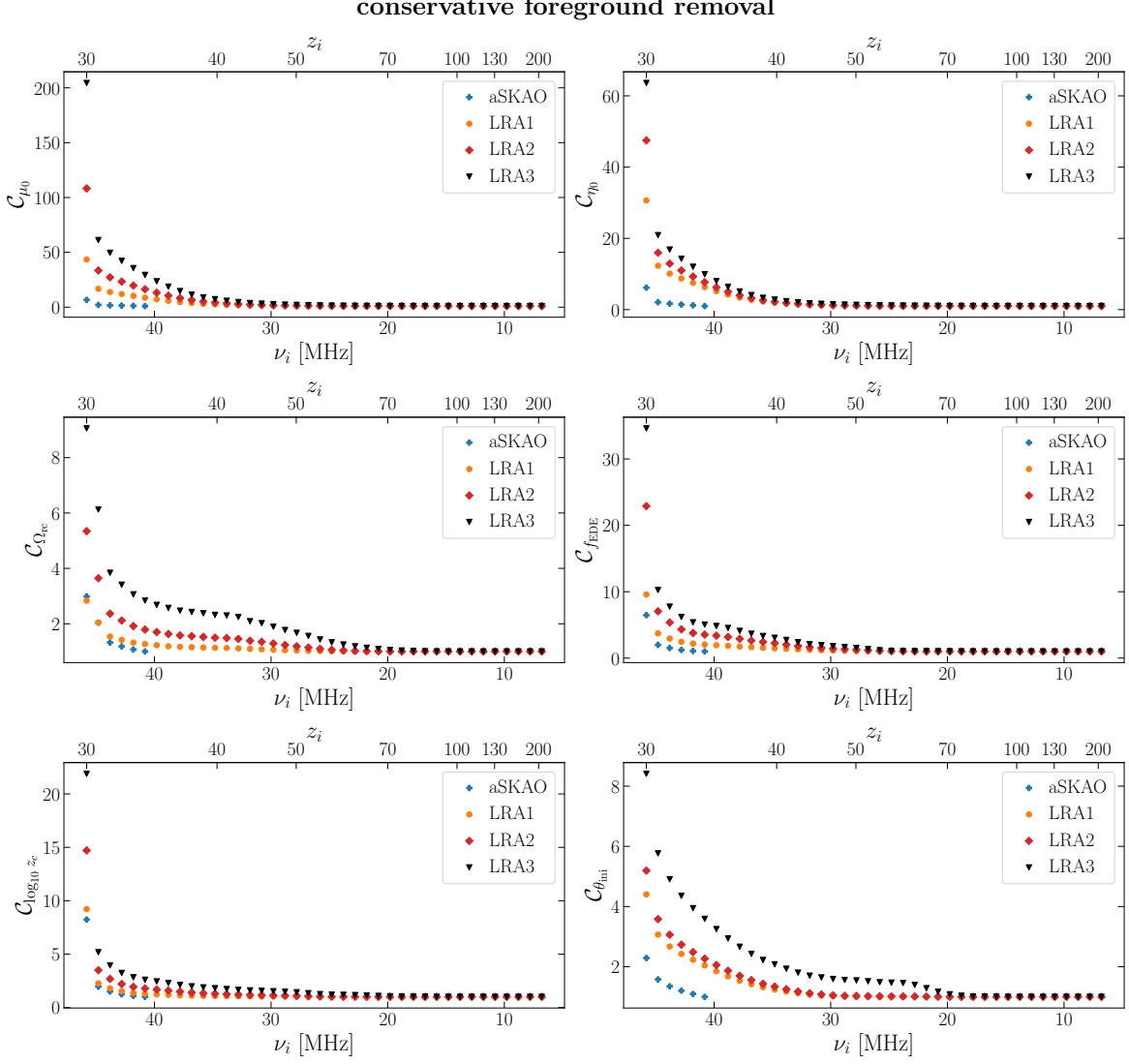


Figure 5: Cumulative error ratio of equation (2.15) obtained by including only the first N frequency bins with respect to the N_ν total number of frequency bins for the parameters of $\mu - \eta$, nDGP and EDE models, employing the conservative foreground removal strategy, see equation (2.17) and the discussion therein. Regarding the $\mu - \eta$ parametrization, we show only the $k_* = 10^{-1} \text{ Mpc}^{-1}$ case since we obtain similar results for all k_* values.

optimistic foreground removal

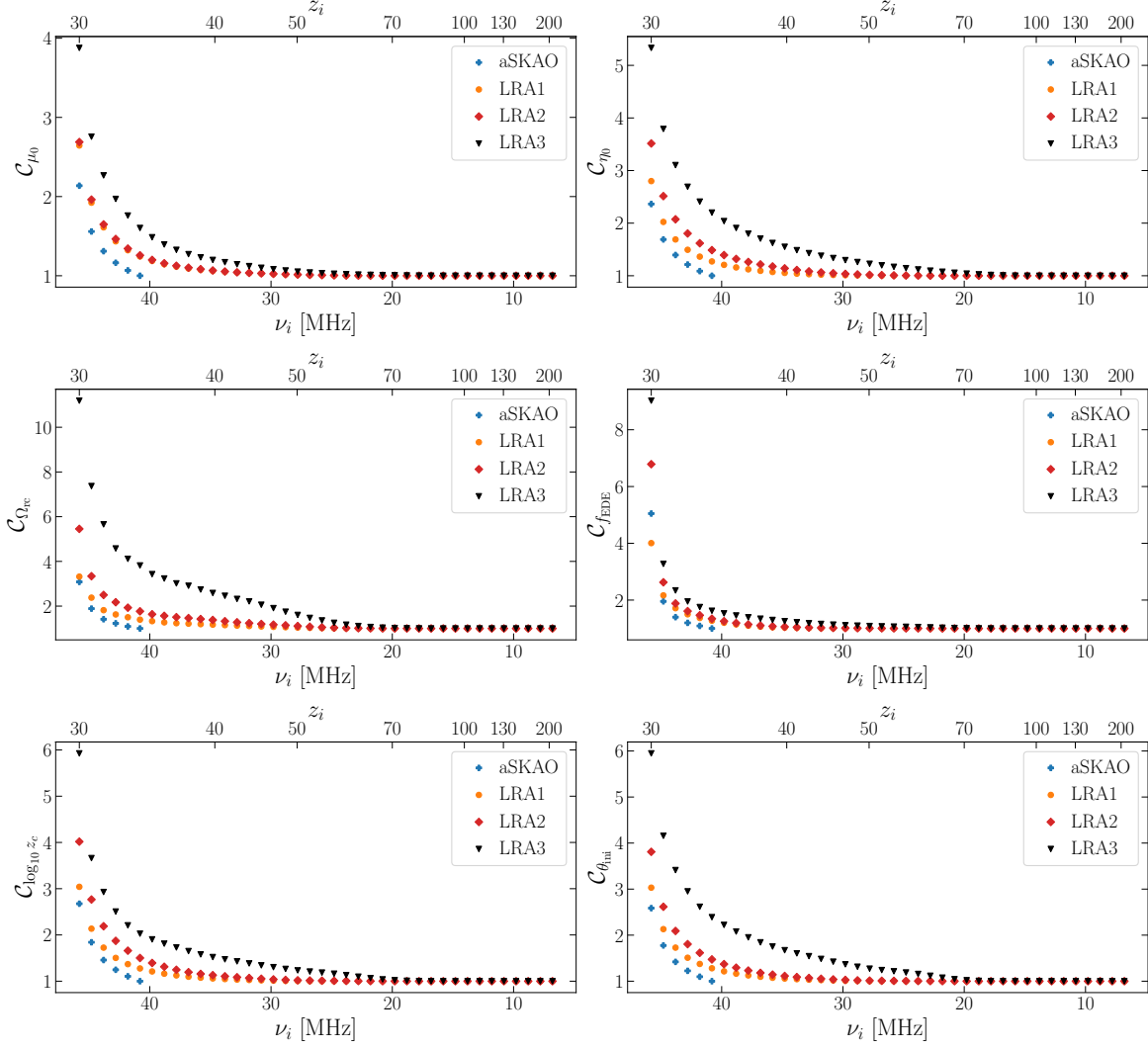


Figure 6: Same as figure 5, but for the optimistic foreground removal strategy, see equation (2.17).

References

- [1] P. J. E. Peebles, “Large-scale background temperature and mass fluctuations due to scale-invariant primeval perturbations”, *The Astrophysical Journal Letters* **263** (Dec, 1982) L1–L5.
- [2] G. R. Blumenthal, S. M. Faber, J. R. Primack, and M. J. Rees, “Formation of galaxies and large-scale structure with cold dark matter”, *Nature* **311** (Oct, 1984) 517–525.
- [3] M. Davis, G. Efstathiou, C. S. Frenk, and S. D. M. White, “The evolution of large-scale structure in a universe dominated by cold dark matter”, *The Astrophysical Journal* **292** (May, 1985) 371–394.
- [4] F. Bernardeau, S. Colombi, E. Gaztañaga, and R. Scoccimarro, “Large-scale structure of the Universe and cosmological perturbation theory”, *Physics Reports* **367** no. 1, (2002) 1–248, [arXiv:astro-ph/0112551](#).
- [5] A. Cooray and R. Sheth, “Halo models of large scale structure”, *Physics Reports* **372** no. 1, (2002) 1–129, [arXiv:astro-ph/0206508](#).
- [6] The **Planck Collaboration**, N. Aghanim *et al.*, “Planck 2018 results - VI. Cosmological parameters”, *A&A* **641** (2020) A6, [arXiv:1807.06209](#).
- [7] S. Aiola *et al.*, “The Atacama Cosmology Telescope: DR4 maps and cosmological parameters”, *Journal of Cosmology and Astroparticle Physics* **2020** no. 12, (Dec, 2020) 047, [arXiv:2007.07288](#).
- [8] Z. Pan *et al.*, “Measurement of gravitational lensing of the cosmic microwave background using SPT-3G 2018 data”, *Phys. Rev. D* **108** (Dec, 2023) 122005, [arXiv:2308.11608](#).
- [9] E. Hawkins *et al.*, “The 2dF Galaxy Redshift Survey: correlation functions, peculiar velocities and the matter density of the Universe”, *Monthly Notices of the Royal Astronomical Society* **346** no. 1, (11, 2003) 78–96, [arXiv:astro-ph/0212375](#).
- [10] M. Tegmark *et al.*, “Cosmological constraints from the SDSS luminous red galaxies”, *Phys. Rev. D* **74** (Dec, 2006) 123507, [arXiv:astro-ph/0608632](#).
- [11] N. P. Ross *et al.*, “The 2dF-SDSS LRG and QSO Survey: the LRG 2-point correlation function and redshift-space distortions”, *Monthly Notices of the Royal Astronomical Society* **381** no. 2, (10, 2007) 573–588, [arXiv:astro-ph/0612400](#).
- [12] J. da Angela *et al.*, “The 2dF-SDSS LRG and QSO survey: QSO clustering and the L–z degeneracy”, *Monthly Notices of the Royal Astronomical Society* **383** no. 2, (12, 2007) 565–580, [arXiv:astro-ph/0612401](#).
- [13] L. Guzzo *et al.*, “A test of the nature of cosmic acceleration using galaxy redshift distortions”, *Nature* **451** (Jan, 2008) 541–544, [arXiv:0802.1944](#).
- [14] C. Blake *et al.*, “The WiggleZ Dark Energy Survey: the growth rate of cosmic structure since redshift $z=0.9$ ”, *Monthly Notices of the Royal Astronomical Society* **415** no. 3, (08, 2011) 2876–2891, [arXiv:1104.2948](#).
- [15] C. Blake *et al.*, “Galaxy And Mass Assembly (GAMA): improved cosmic growth measurements using multiple tracers of large-scale structure”, *Monthly Notices of the Royal Astronomical Society* **436** no. 4, (10, 2013) 3089–3105, [arXiv:1309.5556](#).
- [16] C. Blake *et al.*, “The WiggleZ Dark Energy Survey: joint measurements of the expansion and growth history at $z \lesssim 1$ ”, *Monthly Notices of the Royal Astronomical Society* **425** no. 1, (09, 2012) 405–414, [arXiv:1204.3674](#).
- [17] F. Beutler *et al.*, “The 6dF Galaxy Survey: $z \approx 0$ measurements of the growth rate and σ_8 ”, *Monthly Notices of the Royal Astronomical Society* **423** no. 4, (07, 2012) 3430–3444, [arXiv:1204.4725](#).
- [18] A. G. Sánchez *et al.*, “The clustering of galaxies in the SDSS-III Baryon Oscillation Spectroscopic Survey: cosmological implications of the full shape of the clustering wedges in the data release 10 and 11 galaxy samples”, *Monthly Notices of the Royal Astronomical Society* **440** no. 3, (04, 2014) 2692–2713, [arXiv:1312.4854](#).
- [19] C.-H. Chuang *et al.*, “The clustering of galaxies in the SDSS-III Baryon Oscillation Spectroscopic Survey: single-probe measurements from CMASS anisotropic galaxy clustering”, *Monthly Notices of the Royal Astronomical Society* **461** no. 4, (06, 2016) 3781–3793, [arXiv:1312.4889](#).

- [20] M. Feix, A. Nusser, and E. Branchini, “Growth Rate of Cosmological Perturbations at $z \sim 0.1$ from a New Observational Test”, *Phys. Rev. Lett.* **115** (Jun, 2015) 011301, [arXiv:1503.05945](#).
- [21] T. Okumura *et al.*, “The Subaru FMOS galaxy redshift survey (FastSound). IV. New constraint on gravity theory from redshift space distortions at $z \sim 1.4$ ”, *Publications of the Astronomical Society of Japan* **68** no. 3, (04, 2016) 38, [arXiv:1511.08083](#).
- [22] I. Achitouv, C. Blake, P. Carter, J. Koda, and F. Beutler, “Consistency of the growth rate in different environments with the 6-degree Field Galaxy Survey: Measurement of the void-galaxy and galaxy-galaxy correlation functions”, *Phys. Rev. D* **95** (Apr, 2017) 083502, [arXiv:1606.03092](#).
- [23] S. Alam *et al.*, “The clustering of galaxies in the completed SDSS-III Baryon Oscillation Spectroscopic Survey: cosmological analysis of the DR12 galaxy sample”, *Monthly Notices of the Royal Astronomical Society* **470** no. 3, (03, 2017) 2617–2652, [arXiv:1607.03155](#).
- [24] G.-B. Zhao *et al.*, “The clustering of the SDSS-IV extended Baryon Oscillation Spectroscopic Survey DR14 quasar sample: a tomographic measurement of cosmic structure growth and expansion rate based on optimal redshift weights”, *Monthly Notices of the Royal Astronomical Society* **482** no. 3, (10, 2018) 3497–3513, [arXiv:1801.03043](#).
- [25] S. Nadathur, P. M. Carter, W. J. Percival, H. A. Winther, and J. E. Bautista, “Beyond BAO: Improving cosmological constraints from BOSS data with measurement of the void-galaxy cross-correlation”, *Phys. Rev. D* **100** (Jul, 2019) 023504, [arXiv:1904.01030](#).
- [26] M. Aubert *et al.*, “The completed SDSS-IV extended Baryon Oscillation Spectroscopic Survey: growth rate of structure measurement from cosmic voids”, *Monthly Notices of the Royal Astronomical Society* **513** no. 1, (03, 2022) 186–203, [arXiv:2007.09013](#).
- [27] L. Samushia, W. J. Percival, and A. Raccanelli, “Interpreting large-scale redshift-space distortion measurements”, *Monthly Notices of the Royal Astronomical Society* **420** no. 3, (Mar, 2012) 2102–2119, [arXiv:1102.1014](#).
- [28] A. Raccanelli, D. Bertacca, D. Pietrobon, F. Schmidt, L. Samushia, N. Bartolo, O. Doré, S. Matarrese, and W. J. Percival, “Testing gravity using large-scale redshift-space distortions”, *Monthly Notices of the Royal Astronomical Society* **436** no. 1, (Nov, 2013) 89–100, [arXiv:1207.0500](#).
- [29] D. Huterer *et al.*, “Growth of cosmic structure: Probing dark energy beyond expansion”, *Astroparticle Physics* **63** (Mar, 2015) 23–41, [arXiv:1309.5385](#).
- [30] The **DESI Collaboration**, A. G. Adame *et al.*, “DESI 2024 VII: cosmological constraints from the full-shape modeling of clustering measurements”, *JCAP* **07** (2025) 028, [arXiv:2411.12022](#) [[astro-ph.CO](#)].
- [31] The **DESI Collaboration**, A. G. Adame *et al.*, “DESI 2024 VI: cosmological constraints from the measurements of baryon acoustic oscillations”, *JCAP* **02** (2025) 021, [arXiv:2404.03002](#) [[astro-ph.CO](#)].
- [32] C. Heymans *et al.*, “KiDS-1000 Cosmology: Multi-probe weak gravitational lensing and spectroscopic galaxy clustering constraints”, *A&A* **646** (2021) A140, [arXiv:2007.15632](#).
- [33] The **DES Collaboration**, T. M. C. Abbott *et al.*, “Dark Energy Survey Year 3 results: Cosmological constraints from galaxy clustering and weak lensing”, *Phys. Rev. D* **105** (Jan, 2022) 023520, [arXiv:2105.13549](#).
- [34] L. Verde, N. Schöneberg, and H. Gil-Marín, “A Tale of Many H_0 ”, *Annual Review of Astronomy and Astrophysics* **62** (2024) 287–331, [arXiv:2311.13305](#).
- [35] E. Di Valentino, O. Mena, S. Pan, L. Visinelli, W. Yang, A. Melchiorri, D. F. Mota, A. G. Riess, and J. Silk, “In the realm of the Hubble tension—a review of solutions”, *Class. Quant. Grav.* **38** no. 15, (2021) 153001, [arXiv:2103.01183](#).
- [36] N. Schöneberg, G. F. Abellán, A. P. Sánchez, S. J. Witte, V. Poulin, and J. Lesgourgues, “The H_0 Olympics: A fair ranking of proposed models”, *Physics Reports* **984** (2022) 1–55, [arXiv:2107.10291](#).
- [37] A. R. Khalife, M. B. Zanjani, S. Galli, S. Günther, J. Lesgourgues, and K. Benabed, “Review of Hubble tension solutions with new SH0ES and SPT-3G data”, *JCAP* **04** (2024) 059, [arXiv:2312.09814](#).

- [38] E. D. Kovetz *et al.*, “Line-Intensity Mapping: 2017 Status Report”, [arXiv:1709.09066](#).
- [39] E. D. Kovetz *et al.*, “Astrophysics and Cosmology with Line-Intensity Mapping”, *Bull. Am. Astron. Soc.* **51** no. 3, (2020) 101, [arXiv:1903.04496](#).
- [40] M. B. Silva, E. D. Kovetz, G. K. Keating, A. Moradinezhad Dizgah, M. Bethermin, P. C. Breysse, K. Kartare, J. L. Bernal, and J. Delabrouille, “Mapping large-scale-structure evolution over cosmic times”, *Exper. Astron.* **51** no. 3, (2021) 1593–1622, [arXiv:1908.07533](#).
- [41] K. W. Masui, F. Schmidt, U.-L. Pen, and P. McDonald, “Projected Constraints on Modified Gravity Cosmologies from 21cm Intensity Mapping”, *Phys. Rev. D* **81** (2010) 062001, [arXiv:0911.3552](#).
- [42] P. Bull, P. G. Ferreira, P. Patel, and M. G. Santos, “Late-time cosmology with 21cm intensity mapping experiments”, *Astrophys. J.* **803** no. 1, (2015) 21, [arXiv:1405.1452](#).
- [43] D. Karagiannis, R. Maartens, and L. F. Randrianjanahary, “Cosmological constraints from the power spectrum and bispectrum of 21cm intensity maps”, *JCAP* **11** (2022) 003, [arXiv:2206.07747](#).
- [44] B. R. Scott, K. S. Karkare, and S. Bird, “A forecast for large-scale structure constraints on Horndeski gravity with CO line intensity mapping”, *Mon. Not. Roy. Astron. Soc.* **523** no. 4, (2023) 4895–4908, [arXiv:2209.13029](#).
- [45] S. Casas, I. P. Carucci, V. Pettorino, S. Camera, and M. Martinelli, “Constraining gravity with synergies between radio and optical cosmological surveys”, *Phys. Dark Univ.* **39** (2023) 101151, [arXiv:2210.05705](#).
- [46] E. Castorina and M. White, “Measuring the growth of structure with intensity mapping surveys”, *JCAP* **06** (2019) 025, [arXiv:1902.07147](#).
- [47] A. Moradinezhad Dizgah, E. Bellini, and G. K. Keating, “Probing Dark Energy and Modifications of Gravity with Ground-based millimeter-wavelength Line Intensity Mapping”, *Astrophys. J.* **965** no. 1, (2024) 19, [arXiv:2304.08471](#).
- [48] G. B. Field, “Excitation of the Hydrogen 21-CM Line”, *IEEE Proc.* **46** no. 1, (1958) 240–250.
- [49] M. Zaldarriaga, S. R. Furlanetto, and L. Hernquist, “21 Centimeter fluctuations from cosmic gas at high redshifts”, *Astrophys. J.* **608** (2004) 622–635, [arXiv:astro-ph/0311514](#).
- [50] S. Furlanetto *et al.*, “Astro 2020 Science White Paper: Fundamental Cosmology in the Dark Ages with 21-cm Line Fluctuations”, [arXiv:1903.06212](#).
- [51] P. S. Cole and J. Silk, “Small-scale primordial fluctuations in the 21 cm Dark Ages signal”, *Monthly Notices of the Royal Astronomical Society* **501** no. 2, (11, 2020) 2627–2634, [arXiv:1912.02171](#).
- [52] V. Poulin, T. L. Smith, and T. Karwal, “The Ups and Downs of Early Dark Energy solutions to the Hubble tension: A review of models, hints and constraints circa 2023”, *Phys. Dark Univ.* **42** (2023) 101348, [arXiv:2302.09032](#).
- [53] M. Kamionkowski and A. G. Riess, “The Hubble Tension and Early Dark Energy”, *Ann. Rev. Nucl. Part. Sci.* **73** (2023) 153–180, [arXiv:2211.04492](#).
- [54] G. R. Dvali, G. Gabadadze, and M. Porrati, “4-D gravity on a brane in 5-D Minkowski space”, *Phys. Lett. B* **485** (2000) 208–214, [arXiv:hep-th/0005016](#).
- [55] J. de Kruif, E. Vanzan, K. K. Boddy, A. Raccanelli, and N. Bartolo, “Searching for blue-tilted power spectra in the dark ages”, *Phys. Rev. D* **111** no. 6, (2025) 063507, [arXiv:2408.04991](#) [[astro-ph.CO](#)].
- [56] S. Furlanetto, S. P. Oh, and F. Briggs, “Cosmology at Low Frequencies: The 21 cm Transition and the High-Redshift Universe”, *Phys. Rept.* **433** (2006) 181–301, [arXiv:astro-ph/0608032](#).
- [57] J. R. Pritchard and A. Loeb, “21-cm cosmology”, *Rept. Prog. Phys.* **75** (2012) 086901, [arXiv:1109.6012](#).
- [58] U.-L. Pen, L. Staveley-Smith, J. Peterson, and T.-C. Chang, “First Detection of Cosmic Structure in the 21-cm Intensity Field”, *Mon. Not. Roy. Astron. Soc.* **394** (2009) 6, [arXiv:0802.3239](#).
- [59] T.-C. Chang, U.-L. Pen, K. Bandura, and J. B. Peterson, “Hydrogen 21-cm Intensity Mapping at redshift 0.8”, *Nature* **466** (2010) 463–465, [arXiv:1007.3709](#).

- [60] M. Kuhlen, P. Madau, and R. Montgomery, “The spin temperature and 21cm brightness of the intergalactic medium in the pre-reionization era”, *Astrophys. J. Lett.* **637** (2006) L1–L4, [arXiv:astro-ph/0510814](#).
- [61] A. Pillepich, C. Porciani, and S. Matarrese, “The bispectrum of redshifted 21-cm fluctuations from the dark ages”, *Astrophys. J.* **662** (2007) 1–14, [arXiv:astro-ph/0611126](#).
- [62] A. Lewis and A. Challinor, “The 21cm angular-power spectrum from the dark ages”, *Phys. Rev. D* **76** (2007) 083005, [arXiv:astro-ph/0702600](#).
- [63] Y. Ali-Haïmoud, P. D. Meerburg, and S. Yuan, “New light on 21 cm intensity fluctuations from the dark ages”, *Phys. Rev. D* **89** no. 8, (2014) 083506, [arXiv:1312.4948](#).
- [64] J. B. Muñoz, Y. Ali-Haïmoud, and M. Kamionkowski, “Primordial non-gaussianity from the bispectrum of 21-cm fluctuations in the dark ages”, *Phys. Rev. D* **92** no. 8, (2015) 083508, [arXiv:1506.04152](#).
- [65] R. A. Fisher, “The Fiducial Argument in Statistical Inference”, *Annals Eugen.* **6** (1935) 391–398.
- [66] E. F. Bunn, *Statistical analysis of cosmic microwave background anisotropy*. PhD thesis, University of California, Berkeley, 1995.
- [67] M. S. Vogeley and A. S. Szalay, “Eigenmode analysis of galaxy redshift surveys I. theory and methods”, *The Astrophysical Journal* **465** (1996) 34, [arXiv:astro-ph/9601185](#).
- [68] M. Tegmark, A. N. Taylor, and A. F. Heavens, “Karhunen-Loève Eigenvalue Problems in Cosmology: How Should We Tackle Large Data Sets?”, *The Astrophysical Journal* **480** no. 1, (1997) 22, [arXiv:astro-ph/9603021](#).
- [69] N. Bellomo, J. L. Bernal, G. Scelfo, A. Raccañelli, and L. Verde, “Beware of commonly used approximations. Part I. Errors in forecasts”, *JCAP* **10** (2020) 016, [arXiv:2005.10384](#).
- [70] T. J. Mozdzen, J. D. Bowman, R. A. Monsalve, and A. E. E. Rogers, “Improved measurement of the spectral index of the diffuse radio background between 90 and 190 MHz”, *MNRAS* **464** no. 4, (Feb, 2017) 4995–5002, [arXiv:1609.08705](#).
- [71] A. E. E. Rogers, J. D. Bowman, J. Vierinen, R. Monsalve, and T. Mozdzen, “Radiometric measurements of electron temperature and opacity of ionospheric perturbations”, *Radio Science* **50** no. 2, (2015) 130–137, [arXiv:1412.2255](#).
- [72] A. Liu and J. R. Shaw, “Data Analysis for Precision 21 cm Cosmology”, *Publications of the Astronomical Society of the Pacific* **132** no. 1012, (Apr, 2020) 062001, [arXiv:1907.08211](#).
- [73] A. De Oliveira-Costa, M. Tegmark, B. M. Gaensler, J. Jonas, T. L. Landecker, and P. Reich, “A model of diffuse Galactic radio emission from 10 MHz to 100 GHz”, *Monthly Notices of the Royal Astronomical Society* **388** no. 1, (07, 2008) 247–260, [arXiv:0802.1525](#).
- [74] A. Liu and M. Tegmark, “How well can we measure and understand foregrounds with 21-cm experiments?”, *Monthly Notices of the Royal Astronomical Society* **419** no. 4, (01, 2012) 3491–3504, [arXiv:1106.0007](#).
- [75] H. Zheng *et al.*, “An improved model of diffuse galactic radio emission from 10 MHz to 5 THz”, *Monthly Notices of the Royal Astronomical Society* **464** no. 3, (10, 2016) 3486–3497, [arXiv:1605.04920](#).
- [76] Oppermann, N. *et al.*, “An improved map of the Galactic Faraday sky”, *A&A* **542** (Jun, 2012) A93, [arXiv:1111.6186](#).
- [77] E. R. Switzer and A. Liu, “Erasing the variable: empirical foreground discovery for global 21-cm spectrum experiments”, *The Astrophysical Journal* **793** no. 2, (Sep, 2014) 102, [arXiv:1404.7561](#).
- [78] M. Wolleben *et al.*, “The Global Magneto-Ionic Medium Survey: Polarimetry of the Southern Sky from 300 to 480 MHz”, *The Astronomical Journal* **158** no. 1, (Jul, 2019) 44, [arXiv:1905.12685](#).
- [79] H. K. Vedantham, L. V. E. Koopmans, A. G. de Bruyn, S. J. Wijnholds, B. Ciardi, and M. A. Brentjens, “Chromatic effects in the 21-cm global signal from the cosmic dawn”, *Monthly Notices of the Royal Astronomical Society* **437** no. 2, (11, 2013) 1056–1069, [arXiv:1306.2172](#).

- [80] A. Datta, R. Bradley, J. O. Burns, G. Harker, A. Komjathy, and T. J. W. Lazio, “The effects of the ionosphere on ground-based detection of the global 21-cm signal from Cosmic Dawn and the Dark Ages”, *The Astrophysical Journal* **831** no. 1, (Oct, 2016) 6, [arXiv:1409.0513](#).
- [81] H. K. Vedantham and L. V. E. Koopmans, “Scintillation noise in widefield radio interferometry”, *Monthly Notices of the Royal Astronomical Society* **453** no. 1, (08, 2015) 925–938, [arXiv:1412.1420](#).
- [82] H. K. Vedantham and L. V. E. Koopmans, “Scintillation noise power spectrum and its impact on high-redshift 21-cm observations”, *Monthly Notices of the Royal Astronomical Society* **458** no. 3, (02, 2016) 3099–3117, [arXiv:1512.00159](#).
- [83] J. Lazio, C. Carilli, J. Hewitt, S. Furlanetto, and J. Burns, “The lunar radio array (LRA)”, in *UV/Optical/IR Space Telescopes: Innovative Technologies and Concepts IV*, H. A. MacEwen and J. B. Breckinridge, eds., vol. 7436, p. 74360I, International Society for Optics and Photonics. 2009. <https://doi.org/10.1117/12.827955>.
- [84] A. Datta, J. D. Bowman, and C. L. Carilli, “Bright source subtraction requirements for redshifted 21-cm measurements”, *The Astrophysical Journal* **724** no. 1, (Nov, 2010) 526, [arXiv:1005.4071](#).
- [85] H. Vedantham, N. U. Shankar, and R. Subrahmanyam, “Imaging the epoch of reionization: limitations from foreground confusion and imaging algorithms”, *The Astrophysical Journal* **745** no. 2, (Jan, 2012) 176, [arXiv:1106.1297](#).
- [86] M. F. Morales, B. Hazelton, I. Sullivan, and A. Beardsley, “Four fundamental foreground power spectrum shapes for 21 cm cosmology observations”, *The Astrophysical Journal* **752** no. 2, (Jun, 2012) 137, [arXiv:1202.3830](#).
- [87] A. R. Parsons *et al.*, “A per-baseline, delay-spectrum technique for accessing the 21-cm cosmic ionization signature”, *The Astrophysical Journal* **756** no. 2, (Aug, 2012) 165, [arXiv:1204.4749](#).
- [88] C. M. Trott, R. B. Wayth, and S. J. Tingay, “The impact of point-source subtraction residuals on 12-cm epoch of reionization estimation”, *The Astrophysical Journal* **757** no. 1, (Sep, 2012) 101, [arXiv:1208.0646](#).
- [89] B. J. Hazelton, M. F. Morales, and I. S. Sullivan, “The fundamental multi-baseline mode-mixing foreground in 21 cm epoch of reionization observations”, *The Astrophysical Journal* **770** no. 2, (Jun, 2013) 156, [arXiv:1301.3126](#).
- [90] J. C. Pober *et al.*, “Opening the 21 cm epoch of reionization window: measurements of foreground isolation with PAPER”, *The Astrophysical Journal Letters* **768** no. 2, (Apr, 2013) L36, [arXiv:1301.7099](#).
- [91] A. Liu, A. R. Parsons, and C. M. Trott, “Epoch of reionization window. I. Mathematical formalism”, *Phys. Rev. D* **90** (Jul, 2014) 023018, [arXiv:1404.2596](#).
- [92] A. Liu, A. R. Parsons, and C. M. Trott, “Epoch of reionization window. II. Statistical methods for foreground wedge reduction”, *Phys. Rev. D* **90** (Jul, 2014) 023019, [arXiv:1404.4372](#).
- [93] H.-J. Seo and C. M. Hirata, “The foreground wedge and 21 cm BAO surveys”, *Mon. Not. Roy. Astron. Soc.* **456** no. 3, (2016) 3142–3156, [arXiv:1508.06503](#).
- [94] J. C. Pober *et al.*, “What next-generation 21-cm power spectrum measurements can teach us about the epoch of reionization”, *The Astrophysical Journal* **782** no. 2, (Jan, 2014) 66, [arXiv:1310.7031](#).
- [95] R. Braun, A. Bonaldi, T. Bourke, E. Keane, and J. Wagg, “Anticipated Performance of the Square Kilometre Array – Phase 1 (SKA1)”, [arXiv:1912.12699](#).
- [96] G. Macario *et al.*, “Characterization of the SKA1-Low prototype station Aperture Array Verification System 2”, *Journal of Astronomical Telescopes, Instruments, and Systems* **8** no. 1, (2022) 011014, [arXiv:2109.11983](#).
- [97] J. L. Bernal, A. Raccanelli, L. Verde, and J. Silk, “Signatures of primordial black holes as seeds of supermassive black holes”, *Journal of Cosmology and Astroparticle Physics* **2018** no. 05, (May, 2018) 017, [arXiv:1712.01311](#).
- [98] K. Short, J. L. Bernal, A. Raccanelli, L. Verde, and J. Chluba, “Enlightening the dark ages with dark matter”, *Journal of Cosmology and Astroparticle Physics* **2020** no. 07, (Jul, 2020) 020, [arXiv:1912.07409](#).

- [99] M. McQuinn, O. Zahn, M. Zaldarriaga, L. Hernquist, and S. R. Furlanetto, “Cosmological Parameter Estimation Using 21 cm Radiation from the Epoch of Reionization”, *The Astrophysical Journal* **653** no. 2, (Dec, 2006) 815, [arXiv:astro-ph/0512263](#).
- [100] J. D. Bowman, M. F. Morales, and J. N. Hewitt, “Foreground contamination in interferometric measurements of the redshifted 21 cm power spectrum”, *The Astrophysical Journal* **695** no. 1, (Mar, 2009) 183, [arXiv:0807.3956](#).
- [101] D. Blas, J. Lesgourgues, and T. Tram, “The Cosmic Linear Anisotropy Solving System (CLASS) II: Approximation schemes”, *JCAP* **07** (2011) 034, [arXiv:1104.2933](#).
- [102] L. Amendola *et al.*, “Cosmology and fundamental physics with the Euclid satellite”, *Living Rev. Rel.* **21** no. 1, (2018) 2, [arXiv:1606.00180](#).
- [103] The **Planck Collaboration**, P. A. R. Ade *et al.*, “Planck 2015 results - XIV. Dark energy and modified gravity”, *A&A* **594** (2016) A14, [arXiv:1502.01590](#).
- [104] R. Durrer and R. Maartens, “Dark Energy and Modified Gravity”, 11, 2008. [arXiv:0811.4132](#).
- [105] L. Amendola, M. Kunz, and D. Sapone, “Measuring the dark side (with weak lensing)”, *Journal of Cosmology and Astroparticle Physics* **2008** no. 04, (Apr, 2008) 013, [arXiv:0704.2421](#).
- [106] G.-B. Zhao, T. Giannantonio, L. Pogosian, A. Silvestri, D. J. Bacon, K. Koyama, R. C. Nichol, and Y.-S. Song, “Probing modifications of general relativity using current cosmological observations”, *Phys. Rev. D* **81** (May, 2010) 103510, [arXiv:1003.0001](#).
- [107] D. Alonso, E. Bellini, P. G. Ferreira, and M. Zumalacárregui, “Observational future of cosmological scalar-tensor theories”, *Phys. Rev. D* **95** (Mar, 2017) 063502, [arXiv:1610.09290](#).
- [108] A. Spurio Mancini, R. Reischke, V. Pettorino, B. M. Schäfer, and M. Zumalacárregui, “Testing (modified) gravity with 3D and tomographic cosmic shear”, *Monthly Notices of the Royal Astronomical Society* **480** no. 3, (08, 2018) 3725–3738, [arXiv:1801.04251](#).
- [109] M. Bosi, N. Bellomo, and A. Raccanelli, “Constraining extended cosmologies with GW×LSS cross-correlations”, *Journal of Cosmology and Astroparticle Physics* **2023** no. 11, (Nov, 2023) 086, [arXiv:2306.03031](#).
- [110] E. Bellini and I. Sawicki, “Maximal freedom at minimum cost: linear large-scale structure in general modifications of gravity”, *Journal of Cosmology and Astroparticle Physics* **2014** no. 07, (Jul, 2014) 050, [arXiv:1404.3713](#).
- [111] J. Khoury and A. Weltman, “Chameleon Fields: Awaiting Surprises for Tests of Gravity in Space”, *Phys. Rev. Lett.* **93** (Oct, 2004) 171104, [arXiv:astro-ph/0309300](#).
- [112] J. Khoury and A. Weltman, “Chameleon cosmology”, *Phys. Rev. D* **69** (Feb, 2004) 044026, [arXiv:astro-ph/0309411](#).
- [113] K. Hinterbichler and J. Khoury, “Screening Long-Range Forces through Local Symmetry Restoration”, *Phys. Rev. Lett.* **104** (Jun, 2010) 231301, [arXiv:1001.4525](#).
- [114] P. Brax, C. van de Bruck, A.-C. Davis, B. Li, and D. J. Shaw, “Nonlinear structure formation with the environmentally dependent dilaton”, *Phys. Rev. D* **83** (May, 2011) 104026, [arXiv:1102.3692](#).
- [115] E. Babichev, C. Deffayet, and R. Ziour, “k-Mouflage gravity”, *International Journal of Modern Physics D* **18** no. 14, (2009) 2147–2154, [arXiv:0905.2943](#).
- [116] A. Vainshtein, “To the problem of nonvanishing gravitation mass”, *Physics Letters B* **39** no. 3, (1972) 393–394.
- [117] R. Gregory, N. Kaloper, R. C. Myers, and A. Padilla, “A New perspective on DGP gravity”, *JHEP* **10** (2007) 069, [arXiv:0707.2666](#).
- [118] K. Koyama and R. Maartens, “Structure formation in the Dvali–Gabadadze–Porrati cosmological model”, *Journal of Cosmology and Astroparticle Physics* **2006** no. 01, (Jan, 2006) 016, [arXiv:astro-ph/0511634](#).
- [119] F. Schmidt, “Cosmological Simulations of Normal-Branch Braneworld Gravity”, *Phys. Rev. D* **80** (2009) 123003, [arXiv:0910.0235](#).

- [120] A. Lue, R. Scoccimarro, and G. D. Starkman, “Probing Newton’s constant on vast scales: Dvali-Gabadadze-Porrati gravity, cosmic acceleration, and large scale structure”, *Phys. Rev. D* **69** (Jun, 2004) 124015, [arXiv:astro-ph/0401515](#).
- [121] L. Piga, M. Marinucci, G. D’Amico, M. Pietroni, F. Vernizzi, and B. S. Wright, “Constraints on modified gravity from the BOSS galaxy survey”, *JCAP* **04** (2023) 038, [arXiv:2211.12523](#).
- [122] T. Karwal and M. Kamionkowski, “Dark energy at early times, the Hubble parameter, and the string axiverse”, *Phys. Rev. D* **94** no. 10, (2016) 103523, [arXiv:1608.01309](#).
- [123] V. Poulin, T. L. Smith, T. Karwal, and M. Kamionkowski, “Early Dark Energy Can Resolve The Hubble Tension”, *Phys. Rev. Lett.* **122** no. 22, (2019) 221301, [arXiv:1811.04083](#).
- [124] M.-X. Lin, G. Benevento, W. Hu, and M. Raveri, “Acoustic Dark Energy: Potential Conversion of the Hubble Tension”, *Phys. Rev. D* **100** no. 6, (2019) 063542, [arXiv:1905.12618](#).
- [125] T. L. Smith, V. Poulin, and M. A. Amin, “Oscillating scalar fields and the Hubble tension: a resolution with novel signatures”, *Phys. Rev. D* **101** no. 6, (2020) 063523, [arXiv:1908.06995](#).
- [126] A. C. Sobotka, A. L. Erickcek, and T. L. Smith, “Signatures of very early dark energy in the matter power spectrum”, *Phys. Rev. D* **111** no. 12, (2025) 123522, [arXiv:2409.06778](#).
- [127] D. J. E. Marsh, “The Axiverse Extended: Vacuum Destabilisation, Early Dark Energy and Cosmological Collapse”, *Phys. Rev. D* **83** (2011) 123526, [arXiv:1102.4851](#).
- [128] R. Hlozek, D. Grin, D. J. E. Marsh, and P. G. Ferreira, “A search for ultralight axions using precision cosmological data”, *Phys. Rev. D* **91** no. 10, (2015) 103512, [arXiv:1410.2896](#).
- [129] D. J. E. Marsh, “Axion Cosmology”, *Phys. Rept.* **643** (2016) 1–79, [arXiv:1510.07633](#).
- [130] J. C. Hill, E. McDonough, M. W. Toomey, and S. Alexander, “Early dark energy does not restore cosmological concordance”, *Phys. Rev. D* **102** no. 4, (2020) 043507, [arXiv:2003.07355](#).
- [131] F. Avila, A. Bernui, A. Bonilla, and R. C. Nunes, “Inferring $S_8(z)$ and $\gamma(z)$ with cosmic growth rate measurements using machine learning”, *Eur. Phys. J. C* **82** no. 7, (2022) 594, [arXiv:2201.07829](#).
- [132] O. Doré *et al.*, “Cosmology with the SPHEREx All-Sky Spectral Survey”, [arXiv:1412.4872](#).
- [133] O. Doré *et al.*, “Science Impacts of the SPHEREx All-Sky Optical to Near-Infrared Spectral Survey: Report of a Community Workshop Examining Extragalactic, Galactic, Stellar and Planetary Science”, [arXiv:1606.07039](#).
- [134] O. Doré *et al.*, “Science Impacts of the SPHEREx All-Sky Optical to Near-Infrared Spectral Survey II: Report of a Community Workshop on the Scientific Synergies Between the SPHEREx Survey and Other Astronomy Observatories”, [arXiv:1805.05489](#).
- [135] D. Spergel *et al.*, “Wide-Field Infrared Survey Telescope-Astrophysics Focused Telescope Assets WFIRST-AFTA 2015 Report”, [arXiv:1503.03757](#).
- [136] D. J. Schlegel *et al.*, “Astro2020 APC White Paper: The MegaMapper: a $z > 2$ Spectroscopic Instrument for the Study of Inflation and Dark Energy”, *Bull. Am. Astron. Soc.* **51** no. 7, (2019) 229, [arXiv:1907.11171](#).
- [137] D. J. Schlegel *et al.*, “The MegaMapper: A Stage-5 Spectroscopic Instrument Concept for the Study of Inflation and Dark Energy”, [arXiv:2209.04322](#).
- [138] R. Content *et al.*, “SIRMOS: NIR spectroscopy of 131,000,000 galaxies over $1 < z < 4$ and R 1300”, in *Space Telescopes and Instrumentation 2024: Optical, Infrared, and Millimeter Wave*, L. E. Coyle, S. Matsuura, and M. D. Perrin, eds., vol. 13092, p. 130920Z, International Society for Optics and Photonics. 2024.
- [139] The **Euclid Collaboration**, N. Frusciante *et al.*, “Euclid: Constraining linearly scale-independent modifications of gravity with the spectroscopic and photometric primary probes”, *A&A* **690** (2024) A133, [arXiv:2306.12368](#).
- [140] The **Euclid Collaboration**, B. Bose *et al.*, “Euclid preparation - XLIV. Modelling spectroscopic clustering on mildly nonlinear scales in beyond- Λ CDM models”, *A&A* **689** (2024) A275, [arXiv:2311.13529](#).

- [141] E. McDonough, J. C. Hill, M. M. Ivanov, A. La Posta, and M. W. Toomey, “Observational constraints on early dark energy”, *Int. J. Mod. Phys. D* **33** no. 11, (2024) 2430003, [arXiv:2310.19899](#).
- [142] T. Venumadhav, L. Dai, A. Kaurov, and M. Zaldarriaga, “Heating of the intergalactic medium by the cosmic microwave background during cosmic dawn”, *Phys. Rev. D* **98** (Nov, 2018) 103513, [arXiv:1804.02406](#).